NASA/CR—2007-214685

Adhesion of Lunar Dust

Otis R. Walton
Grainflow Dynamics, Inc., Livermore, California

April 2007

NASA STI Program . . . in Profile

Since its founding, NASA has been dedicated to the advancement of aeronautics and space science. The NASA Scientific and Technical Information (STI) program plays a key part in helping NASA maintain this important role.

The NASA STI Program operates under the auspices of the Agency Chief Information Officer. It collects, organizes, provides for archiving, and disseminates NASA's STI. The NASA STI program provides access to the NASA Aeronautics and Space Database and its public interface, the NASA Technical Reports Server, thus providing one of the largest collections of aeronautical and space science STI in the world. Results are published in both non-NASA channels and by NASA in the NASA STI Report Series, which includes the following report types:

- TECHNICAL PUBLICATION. Reports of completed research or a major significant phase of research that present the results of NASA programs and include extensive data or theoretical analysis. Includes compilations of significant scientific and technical data and information deemed to be of continuing reference value. NASA counterpart of peer-reviewed formal professional papers but has less stringent limitations on manuscript length and extent of graphic presentations.

- TECHNICAL MEMORANDUM. Scientific and technical findings that are preliminary or of specialized interest, e.g., quick release reports, working papers, and bibliographies that contain minimal annotation. Does not contain extensive analysis.

- CONTRACTOR REPORT. Scientific and technical findings by NASA-sponsored contractors and grantees.

- CONFERENCE PUBLICATION. Collected papers from scientific and technical conferences, symposia, seminars, or other meetings sponsored or cosponsored by NASA.

- SPECIAL PUBLICATION. Scientific, technical, or historical information from NASA programs, projects, and missions, often concerned with subjects having substantial public interest.

- TECHNICAL TRANSLATION. English-language translations of foreign scientific and technical material pertinent to NASA's mission.

Specialized services also include creating custom thesauri, building customized databases, organizing and publishing research results.

For more information about the NASA STI program, see the following:

- Access the NASA STI program home page at *http://www.sti.nasa.gov*

- E-mail your question via the Internet to *help@sti.nasa.gov*

- Fax your question to the NASA STI Help Desk at 301–621–0134

- Telephone the NASA STI Help Desk at 301–621–0390

- Write to:
  NASA Center for AeroSpace Information (CASI)
  7115 Standard Drive
  Hanover, MD 21076–1320

NASA/CR—2007-214685

Adhesion of Lunar Dust

Otis R. Walton
Grainflow Dynamics, Inc., Livermore, California

Prepared under Contract NNC06VC87P

National Aeronautics and
Space Administration

Glenn Research Center
Cleveland, Ohio 44135

April 2007

Level of Review: This material has been technically reviewed by NASA technical management.

Available from

NASA Center for Aerospace Information
7115 Standard Drive
Hanover, MD 21076–1320

National Technical Information Service
5285 Port Royal Road
Springfield, VA 22161

Available electronically at http://gltrs.grc.nasa.gov

Adhesion of Lunar Dust

Otis R. Walton
Grainflow Dynamics, Inc.
Livermore, California 94550

Abstract

Lunar dust is a potential problem for planned robotic and manned lunar missions and future in-situ resource utilization (ISRU) operations. This paper reviews the physical characteristics of lunar dust and the effects of various fundamental forces acting on dust particles on surfaces in a lunar environment. In addition to mechanical forces (i.e., from rover wheels, astronaut boots, and rocket engine blast) static electric effects (from UV photo-ionization and/or triboelectric charging) are likely to be the major contributors to the *motion* of dust particles. If fine regolith particles are deposited on a surface, then surface energy related (e.g., van der Waals) adhesion forces, and static-electric-image forces are likely to be the strongest contributors to *adhesion*. Static-image forces at contact scale with the square of the particles' charge and inversely with the square of the particles' size (or the size of charge patches for nonuniform distributions of charge). The typical charge on particles coming from a lunar surface existing at a nearly uniform potential is expected to vary directly with the particle size. The image-charge force for such charged particles contacting a conductive surface would then depend primarily on the square of the particles' surface potential and be nearly independent of their size (e.g., the image-force would be constant, on the order of 0.05 nN/V^2). On the other hand, electrically levitated dust particles may attain net charges (from UV photo-ionization and neutralization by capture of electrons from the plasma sheath) which depend on the square of the particle size. Depending on whether the typical electric charge on fine particles exposed to lunar conditions scales linearly in proportion to the particles' size (i.e., with particle-capacitance, and lunar surface potential) or with the square of the particle size, will determine whether static-image forces *dominate* over surface energy forces, or whether they are *insignificant* compared to surface energy forces, as the size of particles decreases to micron-scale and smaller. Considerable uncertainty also exists in estimates of the magnitude of surface-energy-related adhesive forces, because the lunar environment may allow effective surface energies to be significantly higher than are typically observed in a terrestrial laboratory atmosphere where adsorbed gas molecules can lower the effective surface energy. Also, the short-range nature of van der Waals forces makes them very sensitive to parameters such as the surface roughness of the particles (and the substrate) and the potential existence of ultra-fine particles adhering to larger dust particle surfaces. Typical centrifuge or AFM measurements of particle adhesion forces with nonideal particles and/or surfaces (e.g., rough surfaces) are usually an order of magnitude or so less than theoretically predicted adhesion values. Suggestions for improvements in particle-scale numerical models (DEM) to make them capable of performing sensitivity studies of particle adhesion and removal are offered. Some of the dust removal methods presented at NASA's Dust Workshop (Golden, Colorado, May 2005) are also briefly described, with a note that the CO_2-snow method (used for precision cleaning by the electronics industry) may offer a robust method of "gently" delivering particle-removal forces to micron-scale dust on surfaces in a lunar environment.

Introduction/Background

Recent realization that a very dilute levitated layer of fine charged dust particles is likely in motion above the lunar surface (especially near the terminator), and thus will deposit dust on any surface encountered, means that even surfaces not in contact with the lunar soil, and far from man-made disturbances, will likely acquire layers of dust over time. While electrostatic forces may be the primary driver for dust to be in motion, more than just electrostatics is involved in the adhesion of fine dust

particles to surfaces; both van der Waals forces and the distribution of charge in localized charge "patches" on particles' surfaces have strong influences on particle adhesion.

While some forces that affect fine particles are reduced on the moon relative to their usual terrestrial values (e.g., gravity is reduced by a factor of six, and aerodynamic drag is almost nonexistent), the opposite is true for others. Photoelectric ionization from solar UV radiation, and electron-bombardment from the solar wind, combined with low regolith conductivity, results in the entire lunar surface being charged to a potential of at least several volts in magnitude (positive on the lit side and negative on the dark side). Likewise, the hard vacuum conditions of the lunar environment can result in effective surface energy values being up to two orders of magnitude greater than they would be in humid air at one-atmosphere pressure.

Lunar Regolith

Most of the lunar surface is covered with regolith, a mixture of fine dust and rocky debris produced by meteor impacts and varying in thickness from about 5 m on mare surfaces to about 10 m on highland surfaces. The bulk of the regolith is a fine gray soil with a bulk density of about 1.5 g/cm^3, but it also contains breccia and rock fragments from the local bed rock [Carrier et al., 1991; Todd, 2004; and Taylor et al., 2005]. The large number of very fine particles increases the surface area per unit mass, and thus the surface energy per unit mass available for cohesive forces to act in the bulk material. Also, the absence of air and water has allowed the fines to remain in the regolith as a greater percentage of the mass than would be typical of terrestrial geologic deposits. Chapter 9 of *The Lunar Sourcebook* [Carrier et al., 1991] states that "roughly 10 to 20 percent of the [lunar] soil is finer than 20 μm, and a thin layer of dust adheres electrostatically to everything that comes in contact with the soil: spacesuits, tools, equipment, and lenses. In general, the particles are somewhat elongated and are angular to sub-angular." The specific gravity of the grains in lunar soils "range from 2.3 to >3.2," with a "recommended value of 3.1 for general scientific and engineering analysis of lunar soils." The median size of submillimeter lunar soils ranges from 40 to 130 μm, with an average of 70 μm, and the size distribution is reasonably well represented by a nearly-straight line on a log-normal graph. Fully 25 percent of the mass of Apollo 17 soil sample 78221,8 was comprised of particles smaller than 20 μm, with a few percent smaller than 2 μm.

Adhesion-Related Material Properties, Environmental Conditions, and Scaling Relations

Cohesive forces of attraction between adjacent particles arise from the same physical phenomena as adhesion forces holding fine particles on surfaces. Interparticle cohesion is the major cause of, but is distinct from, the cohesive strength of bulk powders. Appendix A describes what is usually meant by *bulk powder cohesive strength*, and also describes some index tests used to rank powders according to their *cohesivity* or *flowability* (properties which are much less precisely defined). The primary focus of this review is intended to be on factors which affect adhesion of fine particles on surfaces; nonetheless, powder cohesion involves very closely related phenomena. Thus appendix A has been included to clarify the meaning of expressions related to *powder cohesion*.

Surface Energy

Surface energy (per unit area) is the work required to separate a unit area of two surfaces which are initially in intimate contact (on a molecular scale), and move them apart (doing work against the intermolecular forces of attraction) until the surfaces are infinitely far apart. Israelachvili [1991] provides a thorough discussion of interaction energies between molecules and evaluation of the integrated effects of intermolecular interactions between all molecules in each of two spherical or planar objects separated a distance, s, apart (with particular emphasis on the case where the intermolecular potential varies with d^{-6},

where d is the distance between a pair of interacting molecules). One of the more interesting relations cited by Israelachvili comes from the work of Derjaguin [1934] relating the force $F(s)$ on a sphere of radius, R, a distance, s, from a plane of the same material, and the work, $W(s)$, required to separate a unit area of two planes to the same distance, s,

$$F(s)_{\text{sphere}} = -2\pi R W(s)_{\text{plane}} \tag{1}$$

Thus, the cohesive force acting on a rigid sphere in "contact" with a plane ($s_o \approx 4$ Å) can be calculated directly from the conventional surface energy per unit area, γ, since the work of adhesion $W(s_o) = 2\gamma$. For a rigid sphere in contact with a planar surface, we have [Derjaguin, 1934],

$$F(s_o)_{\text{sphere}} = -4\pi R \gamma_{\text{plane}} \tag{2}$$

This intimate relation between the planar surface energy per unit area and the cohesive force acting for sphere/plane contacts is one reason that surface energy is such a useful parameter characterizing cohesive forces of macroscopic bodies in contact. Real macroscopic bodies in contact seldom have intimate (i.e., molecular-scale) planar surfaces touching. Instead, multiple surface asperities are in contact; however, each of these asperity-contacts can often be approximated as a sphere-sphere or a sphere-plane contact. The maximum difference between the attractive force for a sphere-sphere or for a sphere-plane contact is a factor of two [Krupp, 1967; Derjagiun, 1934]. Despite Israelachvili's [1991] insistence that a sphere/plane contact can never respond like a plane/plane contact, when significant plastic deformation occurs in the contact region, the material within that region may closely resemble a plane/plane configuration wherein the cohesive force would be determined by the derivative of the energy-displacement relation, $\frac{-\partial W(s)_{\text{plane}}}{\partial s}$, evaluated at contact, $s = s_o$, multiplied by the actual contact area (at the molecular level). For materials interacting with a van der Waals potential, varying with d^{-6}, this results in a force of cohesion at a planar contact (per unit area) of,

$$F_c = -\frac{4\gamma}{s_o} \tag{3}$$

The significance of surface energy to cohesive/adhesive forces is apparent from equations (2) and (3). Refinements to these relations, taking into account elastic and/or plastic deformations in the contact region will be discussed later, but in all cases, the cohesive force at contact is directly proportional to the surface energy per unit area of the materials involved, whether the contact consists of an undistorted sphere touching a plane, a set of nearly spherical asperities in contact, or "flattened" nearly planar sub-regions in the contact area. Various theories differ in their interpretation of the effects of deformations in the contact region, yet all approaches show a direct relationship between the cohesive forces and the surface energy of the materials in contact. Knowledge of the surface energies of materials of interest, and estimates of the true area of contact are the key factors in being able to predict these surface-energy-related adhesive/cohesive forces acting on fine particulates. A variety of methods exist to measure surface energy of solid surfaces and powdered materials. Appendix B describes some of the methods used to assess surface energy of solids and powders utilizing various "probe" liquids or gases. As discussed in more detail later, the relatively short range of surface-energy related forces can lead to significant uncertainty in quantitatively predicting the "real" contact area and the effects of nearby surface regions on the actual force of adhesion for particles. Nonetheless equation (2) can be used to provide an order-of-magnitude estimate of the adhesion forces involved with lunar-dust-sized particles. For a 10 μm diameter sphere ($R = 5\times10^{-6}$ m) in contact with a planar surface (comprised of the same material) with a surface energy of, say ~100 mJ/m^2, equation (2) gives $F_{\text{sphere}} = -4\pi R\gamma \approx 6$ μN. Typical surface energies range from 20 to 2000 mJ/m^2, and for real, uncharged, nonspherical, rough particles, measured individual-

particle pull-off forces are usually significantly less than values predicted by equation (2), often by much more than an order of magnitude.

Vacuum Environment

One of the more challenging uncertainties in attempting to "predict" cohesive/adhesive forces on fine particles in a lunar environment is how to account for the potentially dramatic effect the lunar vacuum can have on various important phenomena. A number of effects are immediately obvious, such as the insignificance of aerodynamic drag forces, lack of permeability concerns, or out-gassing, etc. (except, perhaps, during lunar avalanches when bound solar-wind gas molecules might be released, causing local fluidization). The lack of water vapor or oxygen, can also affect the surface chemistry of many materials. The hard-vacuum above the lunar surface provides no shielding from UV radiation or bombardment by solar wind particles. Also, the surface energy of materials can be dramatically affected by being in a vacuum. When a new surface is created (as by fracturing) in the presence of a foreign vapor, like laboratory air, some adsorption of vapor molecules (e.g., water, or hydrocarbons) can take place on the newly created surface and lower the surface energy from its value in a vacuum [Israelachvili, 1991; Adamson, 1976]. For example, when mica is cleaved in high vacuum the surface energy is $\gamma_s \approx 4500$ mJ/m^2, but when cleaved in humid laboratory air it falls to $\gamma_s \approx 300$ mJ/m^2 [Bailey et al., 1970]. Similarly, it is well known that ultra-clean, metal surfaces can form "cold-welds" when brought in contact and/or when they slide relative to one another under high vacuum conditions. A mono-layer of oxide or other contamination prevents such bonds from forming and also can lower the measured surface energy significantly [Rabinowicz, 1965]. As noted by Israelachvili [1991] "as a general rule of thumb we may say that the van der Waals interaction is dominated by properties of the bulk or substrate materials at large separations and by the properties of the adsorbed layers at separations less than the thickness of the layers. In particular, this means that the adhesion energies [i.e., at contact] are largely determined by the properties of any adsorbed films, even when these are only a monolayer thick." The lack of an atmosphere does not change the fundamental surface energy of the materials; however, the lack of adsorbed molecules like oxygen or water may mean that materials in a lunar environment will have much less surface contamination, and thus, exhibit a much higher effective surface energy than the contaminated surfaces we are used to dealing with terrestrially.

Changes in particle surface energies with vacuum can result in soil mechanics tests of cohesive-strength being different under vacuum than under usual laboratory conditions. Experimentally the cohesion of Lunar soil sample no. 10084–93 from Apollo 11 (sealed under N_2) [Grossman et al., 1970, cited in Lee, 1995] was measured under vacuum of 5×10^{-9} torr, and then exposed to O_2, O_2+3.5% H_2O at 2, 500, and 760 torr, at 27 and 200 °C. Reduction of cohesion after exposure to the vapor was observed in all cases. Similar changes in the cohesive behavior of fine silicate powder was also observed under high vacuum by Salisbury et al. [1964]. Loss of cohesion for silicates was observed in the presence of air but the cohesion was restored when the system was evacuated. Electrostatic effects were demonstrated not to be the cause of the enhanced cohesion under vacuum. These observation should be a warning that cohesion tests and low-stress consolidation tests on lunar soil samples should not be taken as representative of in-situ behavior, unless they are performed under high vacuum conditions.

Scaling Relations (Effect of Particle Size)

One of the aims of this review is to determine under what conditions various forces are likely to dominate in the adhesion of particles to surfaces, especially under ambient lunar conditions. Because of the way surface forces scale relative to body forces and drag forces, surface phenomena are usually expected to dominate at small particle sizes. Gravity and inertial forces (e.g., response to vibration, shaking or acceleration) scale with the mass of an object, $M = \rho V = \rho(4/3)\pi R^3$, where ρ is density (e.g., kg/m^3), V is volume (e.g., m^3) and R is the "radius" of the object (assuming a spherical shape). Thus, as particles decrease in size the force of gravity, and that due to accelerations, will decrease with the cube of

the particle size. The aerodynamic drag at high Reynolds numbers scales with the cross-sectional area of an object in the flow. As particle size decreases high-Reynolds-number drag forces decrease with the square of the particle size. Likewise, the surface area of a particle decreases with the square of its diameter. Thus, we might expect that most surface related phenomena will scale with the square of particle size (like the surface area). In fact, many phenomena, including some surface related ones, decrease more slowly with particle size than the square. Several important phenomena scale nearly linearly with particle size. As particle size decreases, phenomena which scale linearly with size will eventually dominate over phenomena that scale with higher powers of the size (like gravity, inertial forces, or high-Reynolds-number drag forces). Among phenomena that scale linearly with size, other controlling parameters need to be examined in order to determine which will have a greater influence on particle motion or behavior. Among important forces that scale linearly with particle size are the following:

1) Van der Waals force (i.e., dipole-dipole Keesom-orientation, dipole-non-dipole Debye induction, and nonpolar London-dispersion interactions all exhibit intermolecular potentials that vary as $1/d^6$, where d is the distance between molecular *centers*). The resulting inter-particle force arising from the effect of all the molecules in two adjacent spheres of radius R_1 and R_2 is [Krupp, 1967; Derjaguin, 1934]:

$$F_{vdW} = -\frac{A}{6s^2} R^* \tag{4}$$

where:

$$R^* = \frac{R_1 R_2}{R_1 + R_2}$$

A = Hamaker constant (including both dispersion and polar energies)
s = "gap" spacing between sphere surfaces (minimum value, $s_o \sim 4$ Å, at "contact")

As described by equation (4) the van der Waals force acting between two (nearly touching) spherical bodies (or a sphere and a plane), is a net attraction that varies as the inverse second power of the distance between the *centers of the surface molecules* of the nearly-touching bodies. At "contact" the distance between surface molecules centers is approximately 4 Å (or ~0.4 nm). This inverse second power of the *gap spacing* force (e.g., eq. (4)), is a very short-range force compared to typical particle dimensions—falling by two orders of magnitude by the time the surfaces are 40 Å (~4 nm) apart, and by four orders of magnitude by the time they are 40 nm apart. In comparison, an image-charge force for a charged particle near a conducting surface would decrease two orders of magnitude over a separation distance from touching (e.g., 1-diameter) to ten *particle* diameters (a distance of 10 μm for a 1 μm particle, or 100 μm for a 10 μm particle). The image-force from a small patch of concentrated charge on a particle's surface, say 100 nm across, would also decrease more slowly than the van der Waals force. On a 10 μm particle, a 100 nm diameter patch-charge image-force would decreasing two orders of magnitude going from contact with a conductor to a separation distance of approximately 1 μm, according to the models described later. This is 250 times the distance over which van der Waals force would decrease by two orders of magnitude.

2) The electrical capacitance of an isolated conducting sphere is $C = 4\pi\varepsilon_0 R_p$ [Corson and Lorrain, 1962], where ε_o is the permittivity of free space. Thus, the charge carried by a particle with a uniform surface potential, Φ_s, is given by,

$$Q = C\Phi_s = 4\pi\varepsilon_0\Phi_s R_p \tag{5}$$

and, in an electric field, E, the particle will experience a force $F_E = QE$, or

$$F_E = 4\pi\varepsilon_0\Phi_s E R_p \tag{6}$$

[It should be noted that, the static image-charge force, F_I, acting on a charged particle depends on the square of the charge on the particle, and if nonconducting particles carried uniformly distributed surface charges varying with size according to equation (5) and they were in contact with a conducting surface, they would experience an attractive image-charge force of,

$$F_I \approx \pi\varepsilon_0\Phi_S^2 \tag{7}$$

independent of particle size! This is discussed in more detail later.]

3) Triboelectric charging of particles, also appears to scale nearly linearly with the size of particles, which would again, result in a force in an electric field, E, of $F_E = QE$ with the same dependence on particle size as in equation (6). Figure 1 shows the dependence of tribocharge with particle size for simulant JSC–1-Mars-1 particles, each experiencing the same type and duration of repeated contact with a Co surface [from Sternovsky et al., 2002] (see the discussion under *charge distribution on particles*, later, for some possible reasons for this behavior). [Again it should be noted that if charge scales linearly with particle size then static-electric image-forces acting on such charged particles touching conducting surfaces will be nearly independent of particle size.]

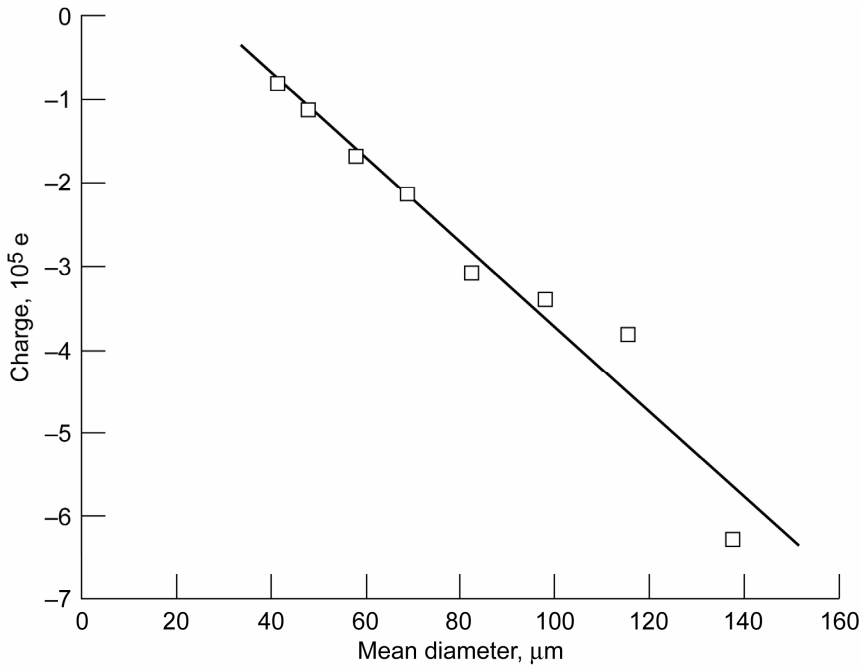

Figure 1.—The charge on JSC–Mars–1 from a contact with a Co surface for different dust sizes.

4) Low-Reynolds-number (i.e., Stokes) drag force:

$$F_d = 6\pi\eta\Delta v R_p \tag{8}$$

where:

η = viscosity of the fluid,
Δv = relative velocity between fluid and particle, and
R_p = particle radius.

Under ambient lunar conditions aerodynamic drag forces are usually negligible (since the only gas present is the occasional vaporized material from a micro-meteorite impact, or the gas escaping when captured solar wind molecules are released as particles fracture). Also, gravity, which is often the primary body force acting on particles, is a factor of six lower on the moon than on earth. Thus, since two of the major forces that might compete with surface forces are greatly reduced from their typical values on earth, and effective surface energies can be higher, we would expect that, under lunar conditions surface phenomena will strongly influence fine particle behavior at even larger sizes than would be the case if the same particulate material existed under one-atmosphere gas pressure on earth.

Electrostatic Charging

Because the minerals comprising the regolith are insulators, and there is no liquid water present, the lunar surface is essentially nonconductive. This means that charges produced on the surface will equilibrate with their external environment and are not conducted to an interior "ground" potential as might occur on earth. During the Apollo explorations scattering of sunlight was observed as a "glow" on the horizon from the dark side of the moon during sunset and sunrise by both surface landers and astronauts in orbit. Subsequent investigations have concluded that electrostatically charged dust grains (possibly in the 5 μm size range and originating from the surface) are the most likely cause of the scattered sunlight [Criswell, 1973]. The Lunar Ejecta and Meteorites (LEAM) experiment was placed on the moon during the Apollo 17 mission to measure high-velocity ejected fine particulates from hypervelocity impacts of micrometeorites on the lunar surface [Berg et al., 1976]. However, most of the impacts recorded were from low velocity, nearly horizontally traveling microparticles, attributed to the transport of electrostatically charged lunar dust. The frequency of the dust impacts was highest when the terminators passed over the detector. Laboratory tests have demonstrated that electric fields from plasma sheaths are capable of levitating small charged particles a few centimeters above a charged lunar stimulant surface [Sickafoose et al., 2002]. Sickafoose et al., also found that fields in the plasma sheath need to exceed a threshold value in order to initiate dust levitation, which they interpreted as being necessary to overcome the surface adhesion of the dust. For lunar-simulant JSC–1 grains, in the size range of 2 to 10 μm, they estimated, based on the charge of the particles and the plasma field available, that the net surface adhesion force they had to overcome in order to initiate levitation was around 5.7×10^{-11} N. (It should be noted that this is on the order of the pull-off van der Waals force expected for a single molecule). Also, Stubbs [2005] has proposed that some very fine lunar dust, with sizes as small as 0.5 μm, may be involved in dilute "dynamic fountains" being lofted 100's of meters above the surface, by the electric field in the plasma sheath, and subsequently falling ballistically back to the moon's surface, where they could be lofted again. In any event, there is ample evidence and speculation that fine dust particles are not merely sitting on the lunar surface as part of the regolith, but that the "ambient" lunar environment includes both a plasma sheath of electrons (on the lit side) and a dilute swarm of fine, charged, dust particles moving and impacting any objects placed on the surface, especially during the passing of the terminator.

Charging of lunar dust particles can come from several sources (and, with no atmosphere, isolated nonconducting regolith particles can maintain a charge once acquired). Photoelectric ionization (from solar UV) on the lit side, and solar-wind electrons on the dark side (in equilibrium with any resulting near-surface plasmas) will result in a nearly uniform surface potential—positive or negative, on the sunlight side or dark side, respectively [Whipple, 1981]. The nearly-uniform lunar surface potentials are expected to result in charges on individual surface particles proportional to the prevailing lunar potential and the capacitances of the particles, $C \approx 4\pi\varepsilon_0 R_p$ (based on a spherical particle of radius R_p). Thus, the net charge attained by regolith particles from these 'solar' sources is expected to depend on their external environment, their photo-ionization efficiencies, and the size of the particles [Sickafoose, et al., 2002; Stubbs et al., 2005; Abbas et al., 2006].

Charge Distribution on Particles

As the terminator passes and the sun rises many UV released photo-electrons will escape into space, resulting in a net positively charged lunar surface. Locally the UV photons typically penetrate less than a micron into the surface particles before being absorbed and potentially "releasing" a photo-electron. Thus, UV-ionization occurs primarily on the sunlit portion of any particles on the lunar surface. Lunar gravity, plus the electric field from the net surface charge of the lunar surface, will provide enough "slowing" to prevent some of the UV-released electrons from escaping into space. The result is that a low-density plasma of electrons (over a height of the Debye length, ~1 m) will shroud the lunar surface. Those electrons in the plasma which reimpact the surface will neutralize some of the positive charges on surface particles. An equilibrium flux of photo-electrons leaving and plasma electrons returning will develop and the plasma will be nearly stable, with slow evolution as the lunar day (fortnight) progresses. The returning plasma electrons will arrive at the lunar surface nearly isotropically from all directions; however, this exchange of electrons with the plasma will likely result in a steady state condition that still leaves the surface particles with a *nonuniform distribution of charge on their surfaces* (because of the asymmetric incident UV photon flux)—even before any tribocharging occurs. Some of the finer charged dust particles will likely become levitated in the plasma sheath. If they remain levitated they will continue to experience photo ionization and canceling interactions with plasma electrons; however, since particle orientations while levitated are continuously changing and random, both the continuing charging and neutralizing effects will be isotropic over the particle surfaces, tending to smooth out any initial nonuniformities in the surface charge distributions of levitated particles. Thus, fine levitated dust particles will be charged, but are likely to have more uniform surface charge distributions than stationary particles comprising the top surface of the lunar regolith, especially if the fine particles have remained levitated for significant periods (e.g., minutes?).

Why does it matter if the surface charge distribution is uniform on dust particles? The distribution of charge on particle surfaces has a significant effect on the electrostatic adhesion of particles to surfaces. As will be described in more detail later, the electrostatic adhesive forces can be an order of magnitude higher if a surface patch of high-surface-charge-density is in contact with (or near) a conducting surface [Hays, 1995; Gady et al., 1996] instead of having that same net charge distributed uniformly over the particle surface.

Recent studies of the photoelectric emission from dust grains exposed to UV radiation [Abbas, et al., 2006] indicate that the photo-electron work function and the threshold energy required for photoelectric emission of an electron from a dust grain are functions of the grain size, and that this dependence extends to larger sizes than previously indicated by the classical image theory equations. As expected, these studies also demonstrated that the photoelectric efficiency, defined as electrons emitted per incident photon, is a function of the particles' charge, or surface potential. The new observation was that this functional dependence is stronger for small grains than for grains of larger sizes. Such grain-size-dependence of the photo-emission efficiency (and/or work function) for UV photoionization, may have a correlation with the size dependence observed for triboelectric charging of dust particles [Sternovsky, et al., 2002] since the tribocharging appears to vary nearly linearly with particle size (see fig. 1) and

effective work function (see fig. 2). Other recent research examining the charging of dust exposed to both UV and electrons [Sickafoose, et al., 2001] indicate charging rates from each effect that are dependent on the particles' surface potential, and thus, likely to scale directly with particle size. It remains somewhat uncertain as to whether the net charge on levitated dust particles will remain distributed directly proportional to the particles' size. Also uncertain is the time evolution of initially nonuniform surface charge distributions on individual particles levitated in a plasma under a high UV flux.

Charging of conductive aerosol water droplets via capture of like-charged ultra-fine particles in the upper reaches of terrestrial thunderstorms results in a maximum charge per droplet that varies approximately with the square of the droplet size [Pruppacher and Klett, 1997, as cited in Tinsley et al., 1999]. The charging mechanisms are different, but not totally distinct from capture of electrons by lunar dust particles levitated in an electron plasma. The charged (conductive) droplet results, and the photo electric emission work of Abbas et al., [2006] raise questions about the likely variation of charge with particle size for levitated dust grains exposed to both continued UV ionization and a dilute flux of electrons from the plasma. Further research may be required in order to establish how the steady-state charge varies with particle size.

The (electron) Work Function—is the minimum energy (usually measured in electron volts) needed to remove an electron from a solid [electrically neutral] to a point immediately outside the solid surface. Here "immediately" means that the final position is far from the surface on the atomic scale, but still close on the macroscopic scale. The magnitude of the work function is usually about a half of the ionization energy of a free atom of the material. [Wikipedia, 2006].

The work function decreases by about a factor of two in going from an isolated atom to a macroscopic surface. Based on classical image theory arguments, it is expected that most of this change occurs in going from a "particle" that is single-atom-size to a nano-scale particle of a few thousand atoms. Recent experiments on photoionization of micron-scale particles, however, indicate that significant size dependence is still in evidence at the micron-scale [Abbas et al., 2006]. It is not entirely clear whether or not buildup of a net charge (and a corresponding surface potential, which would be expected to scale linearly with capacitance, and thus, particle size) may be confounding the size-dependence inferred from such measurements on micron-scale particles. Additional theoretical and experimental research may clarify this issue.

Triboelectric Charging

In addition to the "solar" sources of charging, regolith particles can attain charge through contact electrification (or tribocharging—transfer of charge from one body to another as they touch and come apart). Tribocharging involves the transfer of charge (electrons) from one surface to another in the vicinity of contact. There is little tendency for a statistically-significant net transfer of charge when like-surfaces separate; however, when unlike-surfaces separate a net transfer of electrons from the material with the lower electron-work-function to the material with a higher work-function will occur in the region where the surface separation occurs. Even though there is no *net* transfer of charge, on average, when particles of like material are separated, charge imbalances often occur, so that dispersed particles may carry net charges of either sign, and distributions of charges on individual dust grains can be measured [Muzumder, et al., 1990; 2004] and have been found to vary depending on the method of dispersement. In an open lunar environment nonuniform charge-patches on particle surfaces arising from tribocharging may partially equilibrate due to charge exchange with the plasma and/or those "created" by additional photo-ionization. Tribocharging, and the resulting nonuniform surface-charge distributions on particles, however, could affect attraction and adhesion of particles to rovers, robots, or space suits outside, and on surfaces in any shielded environment. Triboelectric charging is not thoroughly understood, but insulating materials can be classified according to their location in the triboelectric series. This classification is consistent with an ordering according to a material's *electron work function*, ϕ, usually expressed in *eV* [Sternovsky et al., 2002].

Using an apparatus which produced repeated contact and separation of fine particles with metal surfaces in a reproducible manner, along with a technique to capture a stream of the tribocharged particles

in a Faraday cup so that the typical charge-per-particle could be determined, Sternorsky et al., [2002] measured the tribocharging of lunar-dust-simulant JSC–1 due to contact with a variety of metal surfaces. Figure 2 summarizes their results for two particle size ranges on eight metal surfaces (the particle size dependence of mars stimulant JSC–1-Mars was explored using Co—the metal which produced the greatest tribocharging effect on lunar JSC–1, see fig. 1). The four metals with the lowest work functions (i.e., Zr, V, Stainless-steel, and W) are recognized as being subject to oxidation in air, and all behaved in a similar manner (consistent with a work function near 5.6 as expected for oxidized surfaces). The charging from the metals more resistant to oxidation increased monotonically with decreasing work function of the surfaces. As can be seen in figure 2, Sternovsky et al.'s work indicates that the charging rate is directly proportional to the difference in work function, and would thus imply that the average work function of the JSC–1 simulant particles is ~5.9 *eV* (with a slightly lower value for smaller particles, which may have a different mean composition than the larger particles, or might exhibit a different work function simply because of size dependence of that parameter).

While Sternovsky et al.'s work quantifies the work-function for JSC–1 stimulant, it does not provide a value for actual lunar material. Similar measurements (using samples from various locations on the moon's surface, without contamination from exposure to air) would need to be made in order to establish the work-function value for lunar regolith fines. Once typical work-function values are established, then predictions can be made concerning the tribocharging potential from contacts with different materials.

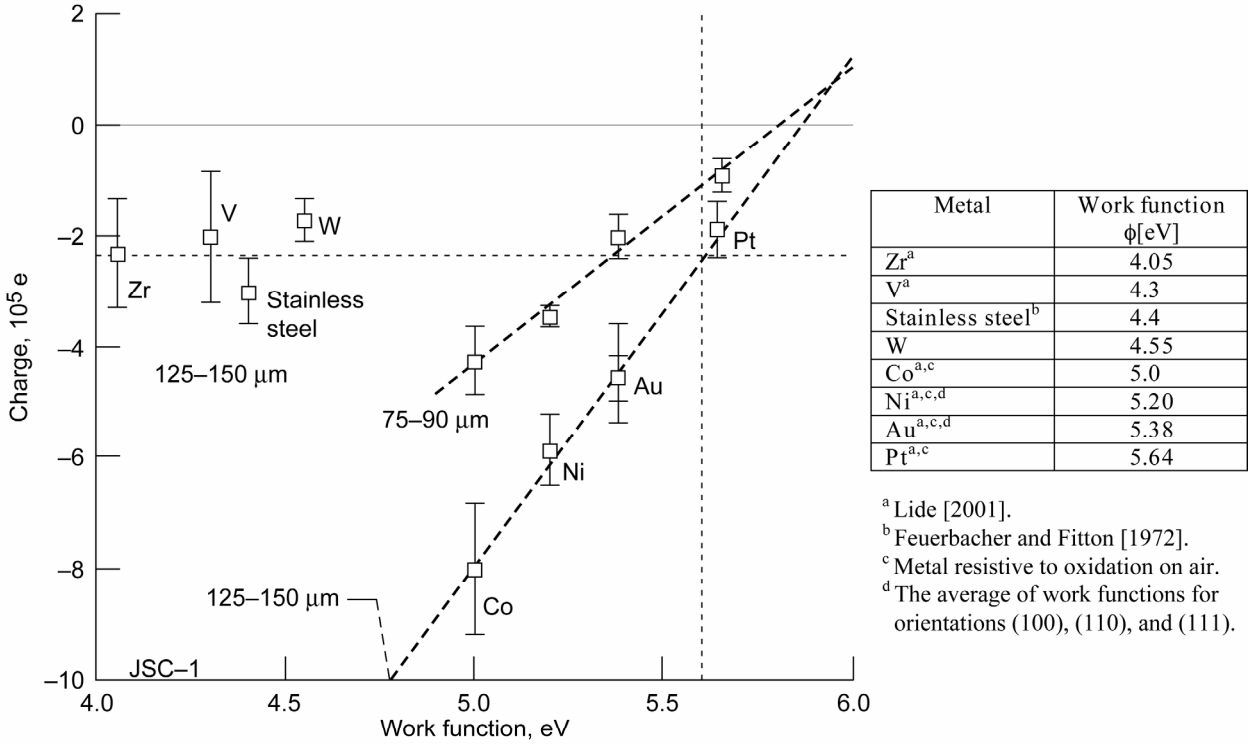

Metal	Work function ϕ[eV]
Zr[a]	4.05
V[a]	4.3
Stainless steel[b]	4.4
W	4.55
Co[a,c]	5.0
Ni[a,c,d]	5.20
Au[a,c,d]	5.38
Pt[a,c]	5.64

[a] Lide [2001].
[b] Feuerbacher and Fitton [1972].
[c] Metal resistive to oxidation on air.
[d] The average of work functions for orientations (100), (110), and (111).

Figure 2.—The charging of lunar dust simulant JSC–1 from different metals [Sternovsky et. al., 2002]. The points represent the average dust charge from six measurements. The dashed lines are the linear regressions calculated for the non-oxidizing surfaces Co, Ni, Au, and Pt. The horizontal dotted line represents the average dust charge from oxidized surfaces. The vertical dotted line indicates the effective work function of oxidized metals.

Xerography

(A technology utilizing tribocharging and electrostatic transfer of fine particles)

Researchers and technologists developing and improving electrophotographic processes (Xerography) have been successfully charging, transporting, removing and precisely depositing 10 μm-scale toner particles onto and off of various surfaces for nearly 50 years. Since its introduction (late 1950s) much of the development in xerographic technology has been by cut-and-try engineering methods. During the last two decades, our understanding of the underlying principles and forces involved in xerography have advanced dramatically, especially with the advent of various surface-force and scanning-probe measurement methods. Nonetheless, a cursory survey of current literature on particle adhesion shows that, even today, several aspects of the process remain incompletely understood. [The following qualitative description, most closely fits the dry-powder xerographic technology of about a decade ago, when it was dominated by black-and-white dry-powder methods, but it still provides insight on methods that have been utilized to "control" electrostatic- and tribocharging of fine particles].

The mechanics of the xerographic process require both electrostatic adhesion/cohesion and interparticle surface-energy-related forces to dominate at different stages. The average surface cohesive forces acting among the toner particles are usually "adjusted" to a fixed (relatively low) value by blending the toner particles with nanoscale (~20 to 40 nm) fumed-silica fines with a weight-fraction of fines in the range of 0.01 to 1 percent. These fines, deposited on the larger-particle surfaces, act as *props* to keep most of the potential surface area at contacts far enough apart that the short-range van der Waals surface forces are greatly reduced. The relatively small contact area of the few propping fines, and the remaining contacting asperities on the particles, provide an appropriate level of cohesion for the process to work.

In xerography the toner particles are triboelectrically charged by mixing with larger carrier beads. The charge on the toner particles enables the electrostatic transfer of these particles between surfaces, allowing the development of an electrostatic latent image and subsequent transfer of the developed image to paper. Because of the requirement for toner transfer, the cohesion and adhesion properties of toner particles are of considerable importance in optimizing the electrophotographic process [Hays, 1995; Pai and Springett, 1993].

In xerography tribocharging is controlled through selection of the material, for the carrier beads (with an appropriate value for its work-function) and toner particles, and by the intensity and duration of "mixing". The surface energy forces are controlled by adjusting the mass fraction of ultra-fine fumed silica blended with the toner; and, the electro-static force is controlled by the electric fields/potentials applied externally. Many of these quantities will be beyond the control of lunar explorers and ISRU designers dealing with fine particles occurring on the moon's surface.

Image Charge Forces from Uniform and Nonuniform Surface Charge Distributions

Many of the potential manmade surfaces anticipated for use on lunar missions are electrically conductive. Thus it is instructive to examine in some detail the forces acting on charged particles near conductive surfaces. When a charged particle is near a conducting surface, the charge on the particle induces a redistribution of charge in the conductor. Because the electric field at the surface of a conductor is always perpendicular to that surface (or there would be currents flowing on the surface), it follows that the potential on that surface is always a constant. That boundary condition can be satisfied by considering the field produced by an "image" charge of opposite sign, located the same distance "inside" the conductor that the center of charge is "above" the surface. By uniqueness, the combined electric field from the primary charge and the image charge correctly describes the electric field in the vicinity of the charge near a conducting surface. The electrostatic Coulomb force acting on a point charge, Q, due to its image "inside" the conductor is

$$F_I = -\frac{QQ'}{4\pi\varepsilon_0 D^2} \tag{9a}$$

where Q' is the image charge (equal in magnitude to Q), and D is the distance between the charge and its image $D = 2d$, where d is the height of the charge above the surface. For a finite-size particle carrying a

charge uniformly distributed on its surface, a similar relation holds, and at "contact" $D \approx 2R_p$. To correctly account for finite sized particles comprised of real dielectric materials the dipole and higher moment distributions induced by the image charge also need to be taken into account. The orientation of the dipoles are such as to increase the attraction due to the monopole terms, so that equation (9a) represents a lower bound on the image charge force on a spherical particle with a uniformly distributed charge Q on its surface (near a conducting surface).

Approximating an irregularly shaped dielectric particle as spherical, and further approximating the additional contribution from polarization with a correction factor, α, the electrostatic image force on the particle contacting a planar, conductive substrate is given approximately by,

$$F_I \approx -\alpha \frac{Q^2}{16\pi\varepsilon_0 R^2} \tag{9b}$$

where Q is the particle charge, R is the average radius, ε_o is the permittivity of free space and α is a correction factor which depends on the polarization of the dielectric particle. (For a dielectric constant of $\kappa = 4$, $\alpha = 1.9$ [Hays, 1988]). For a typical toner particle used in xerography with a charge-to-mass ratio of 15 mC/kg and an average toner diameter of 10 μm, the particle charge, Q is 8fC. The electrostatic image charge as calculated from equation (9b) is ~10 nN. Figure 3 shows measured average toner adhesion forces obtained from centrifuge measurements compared to the image force model calculations (i.e., eq. (9b)) as a function of the average toner charge-to-diameter ratio [Hays, 1994]. The measured values exceed the predictions of the uniform surface charge model by factors of from 5 to 50. The dependence of the measured adhesion on charge ratio eliminates van der Waals adhesion forces as an explanation for the difference, since surface adhesion forces would be independent of charge. (Note that typical toner particles are usually "dusted" with a small quantity of ultra-fine fumed-silica to reduce the van der Waals forces to something on the order of ~10 nN). Hays [1994] proposed that the total charged area A_t on a triboelectrically charged toner particle represents a small part of the total toner particle's surface area. Based on Hays' model, the total charge would be $Q = \sigma A_t$, where σ is the surface charge density (in the charged regions). A small fraction, like 20 percent, of the charged surface area, A_c, might be in close proximity to the conducting surface. If the extent of the charged areas in close proximity, A_c, is much larger than the average distance between the charged surface and the conducting substrate, the magnitude of the electrostatic forces of adhesion can be expressed as, $F_E = -\frac{\sigma^2 A_c}{2\varepsilon_0}$, and the total adhesion can be written as,

$$F_A = -\frac{\sigma^2 A_c}{2\varepsilon_0} - WA_c \tag{10}$$

where WAc represents a nonelectrostatic (i.e., surface-energy based) adhesion contribution. Literature estimates indicate contact charging can produce surface charge densities ranging from 0.5 to 5 mC/m2 depending on the materials involved [Horn and Smith, 1992]. For σ = 1 mC/m2 and Q = 8fC, the electrostatic contribution to the adhesion force is ~100 nN, which is comparable with measured values for toner particles [Hays, 1995].

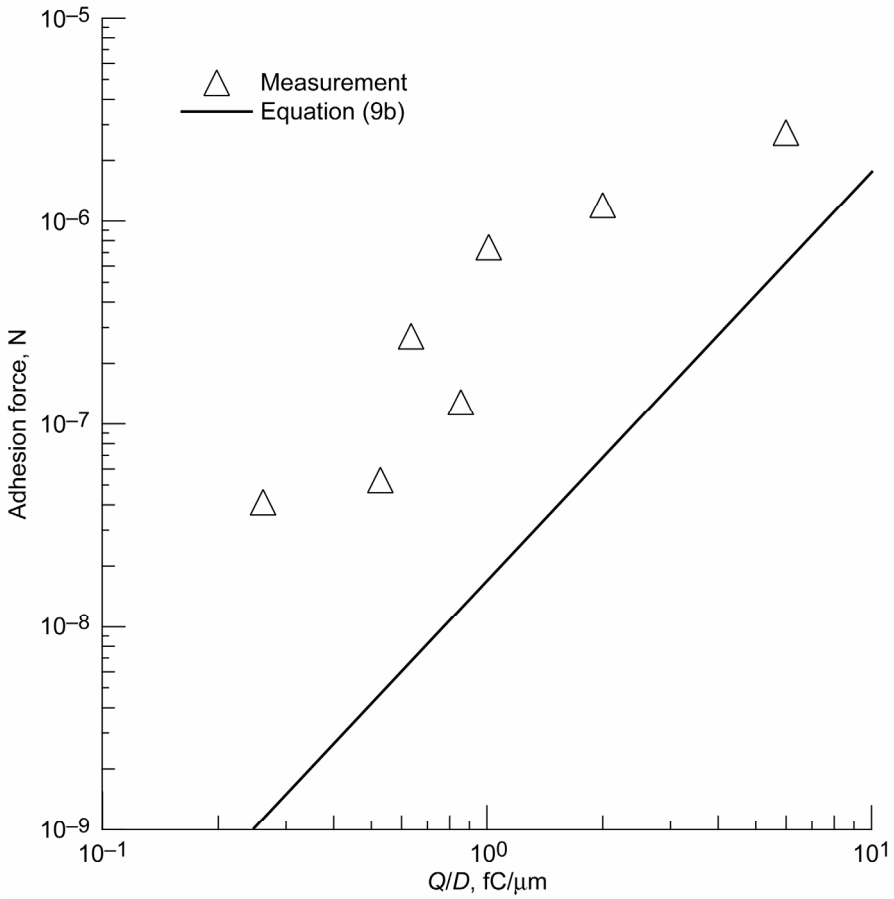

Figure 3.—Toner adhesion forces obtained from centrifuge measurements compared with image force model calculations (eq. (9b)), which assumes charge is distributed uniformly over the particle's surface) as a function of the average toner charge-to-diameter ratio [Hays, 1994].

Gady [1996] performed a series of AFM measurements on 3 and 6 μm polystyrene spheres (attached to an AFM cantilever and) brought toward an atomically flat, highly oriented pyrolytic graphite (HOPG) substrate. Polystyrene and HOPG lie at opposite ends of the tribocharging sequence (i.e., they have large differences in their respective work functions) and thus can produce significant tribocharging upon contact and separation. Gady used the change in frequency of a small driven oscillation of the cantilever to precisely determine the force and force gradient as functions of separation from the substrate. By first contacting the substrate, to establish a precise position for "contact," and then separating the sphere from the substrate and operating in a noncontact mode, Gady was able to map the force-separation relation (until the snap-to-contact point when the sphere was a few nanometers above the surface). Since local charge patches in the region of contact produced high local electric fields (~2.5×10^{8} V/m), these measurements were conducted under a modest vacuum (10^{-2} torr) in order to avoid discharge via breakdown in air. Figure 4 shows a representative force displacement curve for a 3 μm polystyrene sphere. Also shown are theoretical curves for van der Waals force and an electrostatic force based on an assumed charge patch located within a sphere (inside the particle) collocated with the contact spot and having a radius equal to the JKR contact spot radius. The solid line on the figure is the sum of the two theoretical curves. The cross-over point where the van der Waals exceeded the charged-patch electrostatic force (for these highly-charged contacts) varied from 3 to 10 nm depending on the charge on the sphere. At separations closer than the crossover point van der Waals forces dominated the attractive force measured. (Not shown is a curve that would be appropriate for a charge uniformly distributed over the

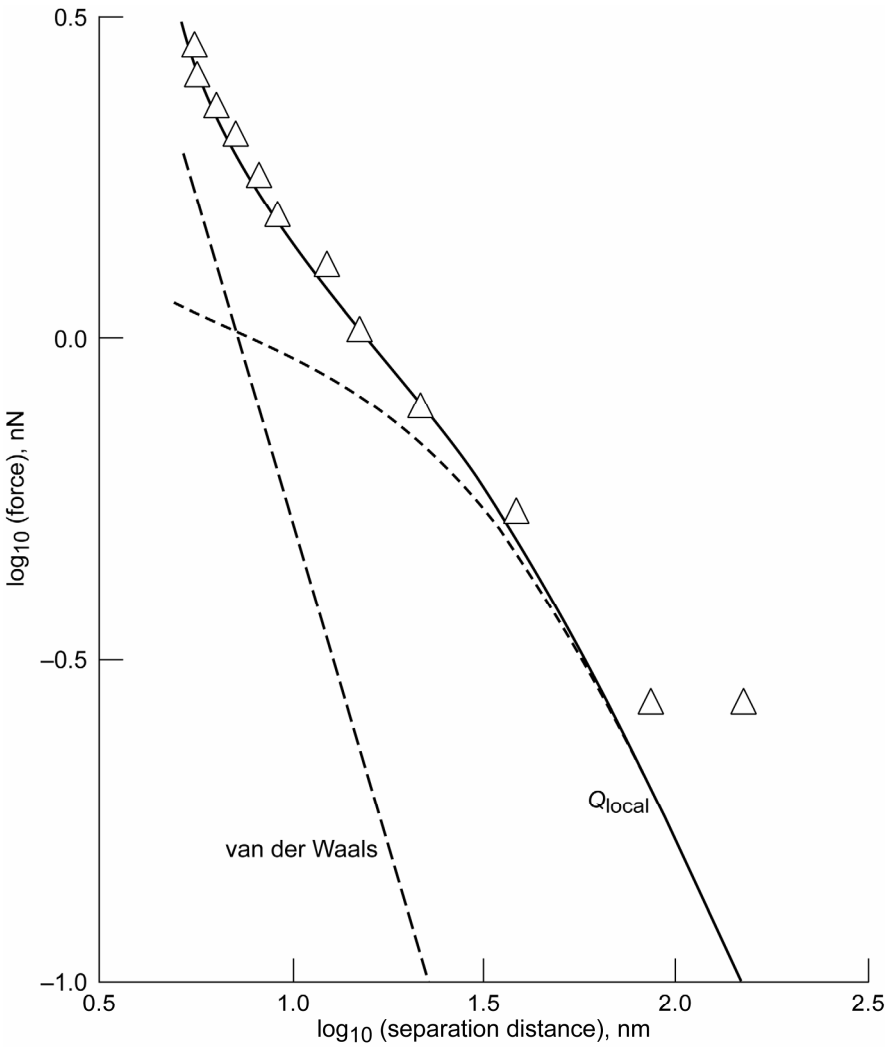

Figure 4.—AMF-measured force-displacement for a triboelectrically charged 3 μm polystyrene sphere near an atomically flat HOPG substrate (symbols), van der Waals force (i.e., eq. (5)) (dashes), and a local charged-patch (of a JKR-contact-spot size) with Q adjusted to best fit the data (dotted line). Solid line is sum of van der Waals and charged- patch curves [Gady et. al., 1997].

surface of the polystyrene sphere. Such a force-displacement curve would be much flatter than the patch-charge curve at close separations). It should be noted that instead of Hays' equation (10) model of a charged-patch force, Gady used a modified form of equation (9a) to generate the Q_{Local} curve, assuming that the local charge Q_L is located in a sphere of radius $R_Q = a$, where a is the JKR contact spot radius. This small "charged sphere" was assumed to be inside of the spherical particle and tangent with the contact spot. This spherical-charged-patch assumption simplified the analysis somewhat, but still captured the physics of having the triboelectric charge located near the contact region.

A more complex mechanism than localized charge-patches, involving a nonuniform distribution of effective work-function values over the surface of particles, has also been proposed as an explanation of the high electrostatic attraction for small charged particles [Pollock, et al., 1994]; however, the simpler localized tribocharged patches as described by Hays [1994] and/or Gady [1996] appear to adequately describe the observed phenomena. In Gady's experiments with spherical particles near a smooth substrate, the van der Waals force did not dominate over image-charge forces until the gap spacing was on the order of 10 nm. Most irregularly shaped particles produced through comminution (as by meteorite

impact on the lunar surface) would have surface roughness at least as great as 10's of nanometers, lowering the effective attraction at contact by an order of magnitude or more.

Range of Effect

The electric field near a large charged surface (like a nearly uniformly charged lunar surface) decreases very slowly with distance away from the surface. Likewise, the static-electric force on a charged particle in such a field (e.g., eq. (6)) also varies slowly with distance. Thus, electrostatic forces have the potential to contribute both as long-range forces affecting *motion* of fine particles and as short-range forces affecting their *adhesion/cohesion*, depending on the net charge on a particle and on the surface charge-density near a contact point. While van der Waals forces, electrostatic image-forces and electrostatic forces between charges, all vary as the inverse square of distance; the distance (of closest approach) differs in each case. As described by equation (4) the net van der Waals force for a single spherical/planar contact (asperity or particle) depends on the distance between the centers of the surface atoms in the two bodies at their point of closest approach. The inverse square relation is not a fundamental property of the dipole forces which comprise the van der Waals interaction. Those forces all decay with the inverse seventh power of the distance on a molecular level. The inverse second power comes from the integrated effect of all (relatively near) atoms in a sphere and in the nearby plane.

Also, at distances greater than approximately 10 nm, retardation effects, of induced dipoles on the molecular level, begin to reduce the effective van der Waals interaction below that predicted by equation (4) (such effects are usually modeled as reductions in the Hamaker constant with distance beyond 10 nm [Israelachvili, 1991]). Thus, for a variety of reasons, surface-energy related adhesion forces are very short range and primarily affect fine particles when they are in contact with each other or touching surfaces. The electrostatic force on the other hand varies as the inverse second power of the distance between the two apparent centers of charge. If we consider the distance over which a force decreases by a fixed factor, say an order of magnitude, below its maximum value at "closest approach," as one measure of the range-of-effect of that force, then we can see significant differences between these three inverse-distance-squared forces. The closest approach values for apparent centers of charge for electrostatic forces are usually much larger than the molecular-scales involved with van der Waals forces, and are more-often on the order of the contact spot size (or asperity height) for triboelectrically charged patches. The image-force for a uniformly charged particle is, in effect, longer-range than the local charged-patch force, which is, in effect, longer-range than the van der Waals force. So, these static-charge forces are less affected by surface asperities and roughness than are van der Waals forces. Thus, for small irregular particles coated with a light dusting of nano-scale fines (as is the case for xerographic toner particles) it is possible for localized charge-patch forces to dominate over van der Waals surface forces in determining the magnitude of particle adhesion. Such may also be the case for small tribocharged lunar dust particles.

Parameters Affecting Surface-Energy Related Adhesive Forces

Van der Waals originally modified the ideal gas equation of state with two additional terms, one to account for the finite volume of the gas molecules and the other to account for an attractive force acting between molecules—which is responsible for liquid/vapor phase changes, among other macroscopic phenomena. For spherical atoms, the van der Waals forces can be thought of as arising from the instantaneous effective dipole of an orbiting electron (and its nucleus) inducing an effective instantaneous dipole in a nearby atom. The resulting dipole-dipole potential energy varies with, $1/d^6$, where d is the distance between the dipole centers of mass. A full quantum mechanical treatment of the energy of different configurations (Feynman *circa* 1939) confirmed that the classical electrodynamic equations were, for the most part, correctly describing these quantum-mechanical atom-atom interactions. Polar molecules (i.e., molecules with a permanent dipole moment) experience this interaction, and also interact via permanent dipole/dipole and dipole/induced-dipole interactions with nearby molecules. These

interactions also have potential energies that vary as $1/d^6$, and are known as the Keesom and Debye energies, respectively. Collectively these three molecular-scale dipole interactions (London-dispersion, Keesom and Debye energy) comprise what are currently known as van der Waals interactions (or forces) between molecules. All molecules (whether they are charged or not, have dipole moments or not, form Hydrogen bonds or not) are attracted to other nearby molecules by, at least the London-dispersion part of, the van der Waals interactions.

Planar Surfaces

Consider a substance comprised of molecules which interact with an attractive pair potential of the form $w(d) = -C/d^6$, where d is the distance between the molecules, and C is a constant. Next, consider a unit area of two planar surfaces, made of that material, which are a distance s apart. If we add all the contributions from all the $1/d^6$ pair interactions, and further integrate the resulting energy with distance, from the distance s to infinity, the result is the surface energy per unit area, as a function of the separation distance between the two planar faces, s, [Israelachvili, 1991]

$$w_p(s) = -\frac{\pi C \rho_a^2}{12 s^2} = -\frac{A}{12\pi s^2} \text{ (per unit area)} \tag{11}$$

where ρ_a is the volume density of atoms (molecules) in the material, and $A = \pi^2 C \rho_a^2$, is the Hamaker constant for the material [Hamaker, 1937].

Spheres

It can be shown that the force, F_s, as a function of separation, s, between two spheres of radii, R_1 and R_2, is related to the surface energy per unit area (as a function of separation) for two planes (i.e., eq. (11)) by [Derjaguin, 1934; Israelachvili, 1991],

$$F_s(s) = -2\pi R^* w_p(s) \tag{12}$$

where, as in equation (4), $$R^* = \frac{R_1 R_2}{R_1 + R_2}$$

If one sphere is very large, $R_2 >> R_1$ (approaching a sphere and a plane) equation (12) reduces to equation (1), or, for two equal spheres

$$F_s(s) = -\pi R w_p(s) \tag{13}$$

For two spheres in contact, where $s \approx s_o$ = molecular diameter, the value of $w(s_o)$ can be associated with 2γ, where γ is the conventional surface energy per unit area of a surface. Thus, the force of adhesion (at contact) between two (undeformed) spheres, in terms of their surface energy is [Israelachvili, 1991],

$$F_s(s_o) = F_{ad} = -4\pi\gamma R^* \tag{14}$$

which reduces to equation (2) if $R_2 >> R_1$, and, for two equal size spheres equation (14) becomes,

$$F_s(s_o) = -2\pi\gamma R \tag{15}$$

Mathematical details of the elastic deformation in the Johnson, Kendall, Roberts (JKR) [1971] model for elastic cohesive contacts are presented in appendix C, along with a discussion of ways various researchers have made modifications to account for plastic deformations in the contact region. The JKR theory for contact forces does not integrate the attractive forces over the two geometries of the contacting bodies, but instead, uses energy arguments and elastic deformation theory to account for the surface energy associated with separating elastically deformable spheres touching over a finite contact area. The model accounts for elastic deformation of the surface both in terms of the repulsive force "flattening" the contact area (similar to a Hertzian elastic contact [Hertz, 1882]), and also a tensile region around the compressively loaded core region, increasing the size of the contact area over a purely compressive, Hertzian deformation. The JKR model predicts a pull-off force value of,

$$F_c = -3\pi\gamma R^* \tag{16}$$

or a 25 percent lower value for the pull-off force over that predicted by equation (14). It is interesting to note that, while the JKR model is based on an analysis that includes elastic deformation of the spheres in the contact region (based on the Young's modulus and Poisson ratio of the material), the final expression for the pull-off force predicted by the JKR model is independent of the elastic constants used to obtain the force-displacement behavior.

When the effects of plastic deformation, such as the flattening of the stress distribution and the widening of the contact area, are taken into account, it is observed that the plastically deformed contact region is "flattened," but is not truly flat. Upon unloading, the region often behaves like an elastic sphere with a larger radius. As the effective radius of the "flattened" area increases, the effective pull-off force increases. By the time significant plastic deformation is occurring in the contact region the effective radius of the contact spot during unloading might be increased by as much as a factor of two. A reasonable approximation of the adhesive-elastic unloading from such a contact is simply a JKR model with a factor of two greater radius of curvature, $R_p \rightarrow 2R$ [Thornton and Ning, 1998]. The net effect is to increase the pull-off force, F_c by up to a factor of two,

$$F_c - \text{plastic} \approx -6\pi\gamma R^* \tag{17}$$

More complex expressions describing the transition from elastic to plastic behavior have also been developed [Margus and Pollock, 1974]; however, the net attraction force is within the bounds already discussed. An additional case, for extremely compliant surfaces, where total particle engulfment is possible, is also discussed briefly in appendix C.

As previously described, the expressions for the adhesive force acting on a spherical particle contacting a planar surface (e.g., eqs. (2), (14), (16) or (17)) would predict a pull-off force of a few microNewtons for a 10 μm diameter particle if the materials involved had surface energies in the range of 40 to 100 mJ/m^2. However, AFM measurements on 8 μm diameter spherical particles (of glass, polystyrene, and tin) contacting atomically flat surfaces resulted in lift-off forces which were typically a factor of 50 less than "predicted" values [Schaefer et al., 1995]. A detailed AFM mapping of the surface asperities and reinterpretation of the contacts as occurring between multiple asperities and the flat substrate, brought the theory and experiments to within a factor of 3 of each other (with the predicted pull-off force still greater than the measured values, but close enough that possible surface contamination could explain most remaining differences). Centrifuge measurements of the average adhesion forces on uncharged irregularly shaped toner particles, of nominally 10 μm diameter, are as high as 50 nN [Hays, 1994] (but nearly two orders of magnitude smaller than would be the case for perfectly smooth spheres of the same size). Also, many irregularly shaped pharmaceutical powder particles, ranging in size from 1 to

200 μm, have been tested on "functionalized" AFM tips by numerous researchers. Generally the (statistical average of the) forces measured, scale directly with the particle size—as expected from JKR (or Derjaguin) theory; and they also, usually scale directly with surface energy (when it has been separately measured). Typical pull-off forces range from 2 to 40 nN for micron-scale particles and from 10's of nN up to ~500 nN for 100 μm scale particles under low humidity [Nagai, 2005]. While no direct measurements of lift-off forces for lunar dust were found in the literature (except the indirect measurement inferred from Sickafoose et al.'s [2002] levitated lunar stimulant tests), the anecdotal evidence is strong that the surface energy related forces will be much smaller that would be predicted from a simplistic application of equation (2), or JKR model pull-off force values, for equivalent-sized spherical particles—primarily because most regolith particles are angular and rough.

Although the descriptions presented in this section have been simplified somewhat and have omitted some mathematical detail, in general, theories for the pull-off forces for sphere-plane or sphere-sphere contacts (including those that account for elastic and plastic deformations in the contact region) give values that are within a factor of two of the expression for nondeformable spherical bodies (e.g., eqs. (2) or (15)). Measured values for adhesion of real micron-scale particles are, more often than not, significantly lower than these theoretical values.

Adhesion-Related Material Properties, Measurements and Representative Values

A variety of theories (applicable for different ranges of particle dimensions, and material properties) have been developed to explain adhesion phenomena. Some assume no deformation and integrate van der Waals forces (e.g., DMT model). Others take into account the elastic and/or plastic deformation of the surfaces (e.g., JKR and MP models, described in appendix C) and require specification of (various subsets of) the following properties:

Particle Radius ..... R
(i.e., radius of curvature in the contact region)
'Work of adhesion' ..... W_a
[$W_a = \gamma_1 + \gamma_2 - \gamma_{12}$, where γ_1 and γ_2 are the two surface energies and γ_{12} is the interfacial energy $\approx \sqrt{\gamma_1 \gamma_2}$].
Electron "Work Function" (to characterize Tribocharging) ..... ϕ
Young's modulus ..... E
Yield strength ..... Y
Poisson ratio ..... ν
Melting temperature ..... T_m

There are several other parameters that could assist in refining estimates of surface forces, *especially information about surface topography, morphology, asperity distributions, etc*., and estimates of particle shape; however, for an initial classification/quantification of adhesion forces the most important parameters appear to be the surface energy, the radius of curvature in the region of contact, the Young's modulus, and the yield strength of the materials of interest. The Poisson ratio is of interest (but can be estimated). The work-function for the material can be useful in determining if tribocharging is likely with various other materials. Rate dependent, viscous and creep effects may also be of concern, especially for plastics or soft polymers; however, the literature for such parameters is mostly anecdotal, with empirically determined time constants used to fit specific cases studied under laboratory conditions. Some quantities, like moduli, strength, and surface energy, change significantly with temperature (especially as melting is approached). Thus, knowing the melting temperature of a material is useful for estimating whether or not the physical properties are likely to be changing significantly with changes of a few hundred degrees in temperature.

Many classes of material have similar values for certain physical properties. For example, all molecules interact via the dispersive part of van der Waals interactions (characterized by the Hamaker constant, A). The surface energies of many materials can be adequately estimated from their Hamaker constants [Israelachvili, 1991]. Metals have surface energies that are determined by the electrons in the conduction band, which behave differently than the orbiting electron-nucleus, instantaneous-dipole model, of the London-dispersion interaction. Metal surface energies are about an order of magnitude higher than would be predicted from their Hamaker constants. Also, the Hamaker constants for metals are about an order of magnitude greater than those of most other materials [Israelachvili, 1991]. The result is that most metals have surface energies that are about two orders of magnitude greater than most nonconducting materials. Materials which form strong covalent bonds are another class with surface energies that cannot be accurately predicted directly from their Hamaker constant values. (This class of materials includes hydrogen-bond forming materials, most organic compounds, as well as materials containing bonds such as Si—O, and F—F) [Israelachvili, 1991].

Rabinowicz [1965] provides many useful general scaling relationships among metal properties, and also for some for nonmetals. For example, for most metals the yield strength is approximately given by

$$Y \approx 0.003E$$

Where, E is Young's modulus. The penetration hardness, p, which Rabinowicz uses to characterize surface deformability, is approximately $p \approx 3Y \approx 0.01E$. Metal surface energies (and surface energies for many nonmetals) appear to scale as the hardness to the 1/3 power (i.e., $\gamma \propto p^{1/3}$). Rabinowicz also utilizes the ratio of surface energy to hardness, γ/p, as a parameter with which to characterize material surfaces, since low values of γ/p are associated with "better" surface interaction behavior for many engineering applications, namely lower friction, smaller wear particles, smoother surfaces, and less adhesion. Figure 5, from Rabinowicz [1965], shows how the adhesive force experienced by spheres pressed into a flat soft metal surface depends on the ratio of work-of-adhesion, W, to hardness, p.

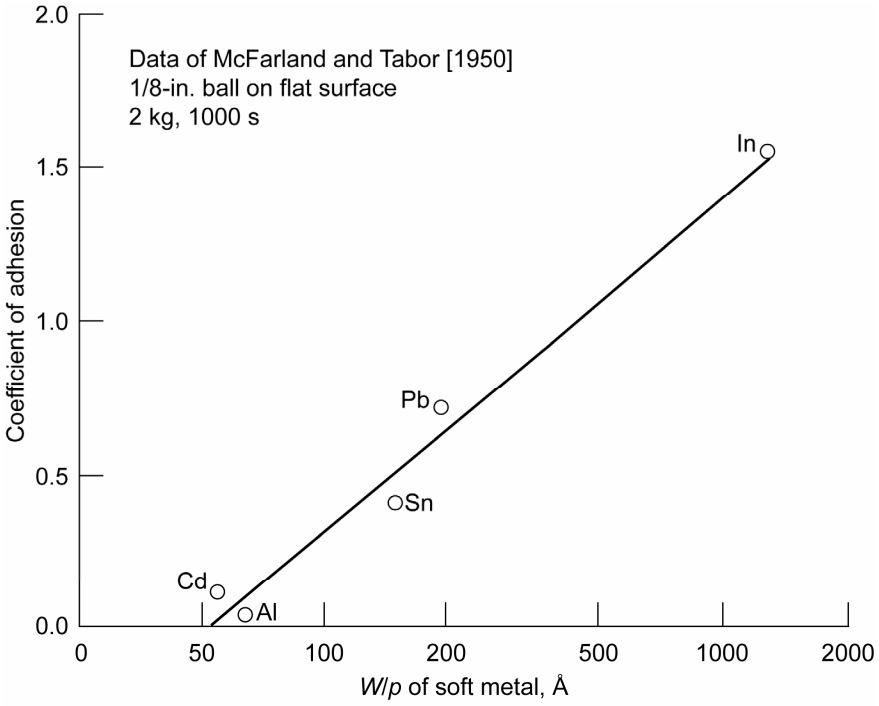

Figure 5.—Adhesion versus the ratio of surface energy to hardness for 1/8 inch spheres pressed into a flat, soft metal surface [Rabinowicz, 1965].

More recent papers on the properties of polymers give similar relations between hardness, yield strength and Young's modulus for those materials. The Young's modulus for polymers is typically around 3 GPa at temperatures below the glassy temperature transition, and drops three orders of magnitude to around 3 MPa above that transition. Upon further temperature increase polymers typically undergo another transition to a terminal state with a very low modulus wherein they appear "tacky". The glass transition temperature of individual polymers can be modified through the addition of a plasticizer, so that the modulus versus temperature properties can be tailored by varying the plasticizer content [Rimai, et al., 1996; van Krevelen, 1976]; however the approximate relation Rabinovicz described for metals, $p \approx 3Y \approx 0.01E$, still holds for each region.

By comparing the cohesive force between two spherical particles (eq. (15), or 3/4 of that value if we use the JKR theory) with the maximum load achievable for elastic spheres in contact before plastic deformation occurs (eq. (C6) in appendix C) we find that as particles get smaller they will eventually reach a size where the cohesive force will cause plastic deformation, even without any applied load (see eq. (C8)). Table 1 shows the particle size (diameter) below which plastic deformation is likely due simply to the cohesional forces for two spheres in contact, without any external loads, for various values of Young's modulus, E, and surface energy, γ (assuming $\nu = 0.3$, and $Y \approx 0.003E$).

TABLE 1.—PARTICLE DIAMETER BELOW WHICH PLASTIC DEFORMATIONS OCCUR AT CONTACTS

E ↓ and γ →	20 mJ/m^2	200 mJ/m^2	2000 mJ/m^2
1 GPa	400 μm	4 mm	40 mm
10 GPa	40 μm	400 μm	4 mm
100 GPa	4 μm	40 μm	400 μm

Discussion

From the works of London, Hamaker, Feynman, Lifshitz, Keesom, Debye and others we have a reasonably good understanding of the molecular-scale sources of van der Waals forces; however, the integrated macroscopic effects of van der Waals forces as described above are only straightforward to calculate for idealized configurations. For most real contacts between macroscopic objects, the adhesive forces can differ substantially from what would appear to be a straightforward integration of a known intermolecular potential over all nearby molecular centers. It is the relatively short-range nature of van der Waals forces (from a macroscopic perspective) which give rise to much of the "uncertainty" in calculating their effects for real macroscopic contacts. As pointed out by Israelachvili [1991] one source of uncertainty in predicting adhesion forces from models of van der Waals interactions is uncertainty associated with the effective surface energy, since even monolayers of gas molecules adsorbed on a surface can affect the value of the adhesive force at contact. Two other factors which contribute significant uncertainty to making quantitative predictions of adhesion forces are *surface morphology* (or roughness), and *deformation* (elastic and plastic) in the contact region. Measurements of pull-off forces for small particles, can be substantially less than the values predicted *a priori* from known surface energies or Hamaker constants for the materials involved, with the over prediction by the theory increasing as the particle size decreases. Large soft spheres, on the other hand, adhere in almost exact agreement with the Johnson, Kendall, Roberts (JKR) theory [1971]. JKR theory accounts for elastic deformation in the contact region, but is still within 30 percent of the Derjagian approximation for undeformed spheres, e.g., equation (2), at contact. Surface roughness (e.g., detailed surface morphology) has been identified as one major contributor to the discrepancy between measured pull off forces for "real" particles and theoretical predictions for smooth surfaces [Rabinovich, et al., 2000 and 2002; Rimai and Quesnel, 2001; Mizes, 1994; Schaefer et al., 1995]. Likewise as the particle size (or the radius of curvature in the contact region) decreases, it is possible for plastic deformations to occur at the contact, even with no external loads; however, plastic deformation are usually expected to cause less than a factor of two increase in effective adhesion forces (unless external loads are also applied to the contacting bodies).

Because of the short-range nature of adhesive surface forces, it can be said with some certainty that adhesive surface forces are likely to be a major concern *only* when attempting to remove particles from surfaces. Under ambient lunar conditions, surface forces will have *only a minimal contribution* as to whether or not particles make contact with surfaces. [This is contrary to the potential effects of surface forces on particles in a third media, like in aqueous suspensions, where net surface forces can have a strong influence on whether "contact" occurs].

Rough estimates of distance ranges over which various force are likely to dominate (for 10-μm-scale particles in a lunar environment) might be summarized as follows, where, s is the distance between a particle and a (conducting) surface:

- $s > 0.1$ μm, electrostatic forces due to the *net charge* on particles dominate
- 100 nm > s >10 nm, electrostatic forces due to localized *charge patches* on particle surfaces may have a significant effect
- $s < 10$ nm, van der Waals (surface energy related) forces may dominate (if surfaces are smooth enough and/or surface energies high enough)

Levitated dust particles, unlike triboelectrically charged particles, may attain nearly uniform charge distributions, eliminating any special consideration for *charge patches* on levitated particle surfaces. Very rough, irregular particles or particles with a dusting of nanoscale fines may have very low van der Waals adhesion forces.

Particle-Scale Simulation Models

Particle-scale numerical simulations of deposition and removal of dust have the potential to allow sensitivity studies to be performed, in order to determine how the variability in an uncertain force-model parameter can affect a proposed dust-mitigation strategy. Unfortunately, the current state-of-the-art in discrete-particle numerical modeling is not quite to the point where such sensitivity studies could provide believable quantitative results for regolith particles with realistic characteristics. Relatively straightforward enhancements to existing models could make them into useful tools for such assessments.

Dozens of particle-scale numerical simulation models (primarily Discrete Element Method, DEM, codes following the spirit of the pioneering work of Cundall and Strack [1979]) have been successfully used to calculate macroscopic granular flows (usually involving millimeter-scale and larger particles) where cohesive-force effects are minimal. Some limited work with cohesive forces has also been done, but primarily for particles of larger size than lunar dust, and seldom including nonspherical shapes or rotational moments at contacts [e.g., Thornton and Ning, 1998]. On the molecular scale, recent improvements in molecular-dynamics modeling and computational power are beginning to allow simulations of such complex phenomena as folding of protein molecules [e.g., Liwo et al., 2005], involving hundreds to thousands of individual atoms. For micron-scale particles (such as might be appropriate for simulating the behavior of lunar dust particles, the bulk deformation of fine regolith aggregates, and removal of dust particles from surfaces) no currently available simulation models include enough realism to be adequate predictive tools. Walton [2004] suggested some improvements to the current state-of-the-art for DEM models for simulating such fine particulates, combining the effects of contact moments with normal and tangential force models for elastic-plastic cohesive contacts. Very few current simulation models include the effects of moments at contacts [notable exceptions include**,** Bartels et al., 2005; Wolf et al., 2005, Hopkins, et al., 2004]. To date Tomas [2006] has described what might be the most complete set of simplified mathematical models likely capable of realistically describing micron-scale particle-particle and particle-surface interactions, including cohesion, moment-torques, and plastic deformation at contacts. To the author's knowledge, Tomas' models are not currently included in any DEM or molecular-dynamics codes used to simulate the behavior of particulate assemblies. In addition to relatively-complete, and quick-to-evaluate, models for contact forces, like those described by Tomas, a particle-scale simulation method aimed a evaluating various strategies for fine-particulate removal from

surfaces would also need to include the effects of potential aerodynamic drag (i.e., gas-particle coupling), electrostatic forces (i.e., long-range forces) and nonuniform distributions of charges on particles and/or surfaces. To date, no such comprehensive particle-scale model exists that incorporates appropriate models of the forces and torques acting on micron-sized regolith particles.

Removal of Dust

A wide variety of cleaning methods exist for removing particles and other contaminates from surfaces. The microelectronics industry, in particular, is especially concerned with removing particles as fine as sub-micron-size from surfaces of silicon. A NASA sponsored workshop (May 2005, Golden, Colorado) identified a wide variety of potential dust mitigation methods for manned lunar and Martian missions. Mitigation techniques identified as having potential for significant benefit included multilevel or multilayer barriers to prevent dust intrusion, electromagnetic "shields" and specialized coatings on surfaces to minimize dust accumulation, and a variety of approaches to remove dust once it is deposited on surfaces.

Removal of particles from a surface requires methods (1) to deliver sufficient force to particles to dislodge them from the surface (e.g., overcome surface energy or electrostatic adhesion forces) and (2) to transport detached particles far enough away from the surface that they do not immediately redeposit. Mechanical vibration requires high frequencies in order to couple to the resonant frequency of attached particles—thus, ultra-sonic baths in liquids have proven effective at fine particle removal. Liquid immersion is not practical, however, for most lunar situations. Also, direct mechanical (i.e., contact) vibration may not be practical for many configurations. A noncontacting electromagnetic "brush" with oscillating EM fields may offer a removal method applicable to a lunar environment, but such a device has yet to be demonstrated to be effective. Mechanical wiping or brushing of surfaces can deliver sufficient force to dislodge particles, but can also cause serious damage to delicate surfaces due to scratching (especially if the particles are hard and angular, like lunar regolith fines). Removable soft, thin films, which can be either mechanically applied, or sprayed on, and pulled off (with motion primarily outward from the substrate) offer an attractive alternative method of removing dust with minimal displacement along the surface (and thus minimal scratching). A major disadvantage of thin-film pull-off methods is the quantity of consumable material used. Blowing high pressure gas over a surface is often ineffective at removing very fine particles (e.g., micron-scale) because the fine particles reside inside the gas-surface boundary layer which has low gas velocity near the surface (and thus minimal "lift" and shear forces on the adhered particles). Adding particles to a high pressure gas stream is a well recognized method for cleaning contaminated surfaces (e.g., media-blasting or sand-blasting). If the "particles" in the gas stream are comprised of evaporable droplets or frozen-gas particles, they offer the added advantages of both disappearing after impact, and providing a "source" of additional gas very near the impacted surface to assist in pneumatically transporting any removed contaminant. That is the theory behind the CO_2-snow cleaning approach, in which compressed CO_2 gas expands in a specially designed expansion-chamber-nozzle, forming nanoscale crystals which aggregate before exiting the nozzle into micron-scale "snow-flakes" in a high velocity CO_2 gas stream, directed at an oblique angle onto a surface to be cleaned (usually with a stand-off distance on the order of a centimeter or so) [web sites for three commercial CO_2 snow suppliers: PurCO_2, Applied Surface Technologies, and Eco-Snow, are listed under their names in the references]. While such a technique requires significant use of a consumable (CO_2 gas or liquid), it is a material readily available on Mars, and in the past, has been discarded from space-based habitat environments (like the ISS). CO_2 snow cleaning is among the methods currently being evaluated by NASA for dust mitigation on future missions (e.g., see: http://see.msfc.nasa.gov/nec/nectech.htm). Nothing found in this study of dust adhesion forces would negate CO_2-snow cleaning as a candidate technique for dust removal.

Concluding Remarks

This review of adhesive forces potentially acting on lunar dust particles leaves many questions unanswered. That was part of its purpose—to highlight where additional research may be needed and to aid in determining the most fruitful areas for development of improved measurement or modeling technologies. Based on the literature examined in this study, answers to the following questions appear that they could significantly influence estimates of adhesive surface forces acting on lunar dust on surfaces (including electrostatics):

1. How is net in-situ charge related to particle size for both levitated dust particles and for particles forming the top layer of the lunar regolith? (If charge scales nearly linearly with size, then the cohesion of the finest particles may be dominated by charge effects in most cases).
2. What is the effective surface energy of typical regolith and what is the influence of lunar conditions (especially high vacuum) on that effective surface energy?
3. How significant of a reduction in particle-surface adhesion forces may result from the combined effects of particle surface- roughness and/or a dusting of ultra-fine material on the micron-scale particles?
4. How significant are nonuniformities in charge distribution on individual dust particle surfaces, after sustained exposure to UV photo-electric ionization and neutralizing plasma-electron fluxes?
5. What is the effective electron work function of typical lunar regolith (and how does it compare to the value of typical manmade materials which will be making repeated contacts with the regolith)?
6. How heterogeneous is the *in situ* distribution of charge on the lunar surface, on the lit and dark sides of the moon and in shadows *versus* areas exposed to direct UV radiation? Answers to these and additional questions await additional research and measurements.

References

Abbas, M.M., D. Tankosic, P.D. Craven, J.F. Spann, A. LeClair, E.A. West, J.C. Weingartner, A.G.G.M. Tielens, J.A. Nuth, R.P. Camata, and P.A. Gerakines, (2006) "Photoelectric emission measurements on the analogs of individual cosmic dust grains," *The Astrophysical Journal*, 645:324–336, July 1.

Abdullah, E.C. and D. Geldart (1999) "The use of bulk density measurements as flowability indicators," *Powder Technol*. 102 151–165.

Adamson, A.W. (1976) *Physical Chemistry of Surfaces*, 3rd ed. Wiley, NY and London, and 5th ed. (1990).

Ahfat, N.M., G. Buckton, R. Burrows, M.D. Ticehurst (2000) "An exploration of inter-relationships between contact angle, inverse phase gas chromatography and triboelectric charging data," *European J. of Pharm. Sci*., 9, 271–276.

Applied Surface Technologies: www.Co2Clean.com New Providence, NJ 07974.

Bailey, A.I., A.G. Price, and S.M. Kay (1970) *Spec. Discuss. Faraday Soc* I, 118–127.

Bartels, G.T., Unger, D., Kadau, D.E. Wolf, and J. Kertész (2005) "The effect of contact torques on porosity of cohesive powders," *Granular Matter*, 7, (2–3), pp. 139–143.

Berg, O.E., Wolf, H., Rhee, J.W. (1976) "Lunar soil movement registered by the Apollo 17 cosmic dust experiment, in Elsässer, H. Fechtig, H. (eds.), Interplanetary Dust and Zodiacal Light, Springer-Verlag, Berlin, pp. 233–237.

Burns, A.R., J.E. Houston, R.W. Carpick, and T.A. Michalske, "Friction and Molecular Deformation in the Tensile Regime," *Phys. Rev. Lett*., 82, 6, p. 1181 (1999).

Carrier, W. David, III, Leslie G. Bromwell, and Martin R. Torrence, (1973) "Behavior of Returned Lunar Soils in Vacuum," *J. Soil Mechanics and Foundations Division, ASCE*, vol. 99, no. SM11, Proc. Paper 10156, Nov. 1973, pp. 979–996.

Carrier III, W.D., G.R. Olhoeft, and W. Mendell (1991) "Chapter 9: Physical Properties of the Lunar Surface," in *Lunar Sourcebook: a User's Guide to the Moon*, G.H. Heiken, D.T. Vaniman, and B.M. French, editors, Cambridge University Press.
Chow, A.H.L., H.H.Y. Tong, B.Y. Shekunov, P. York (2004) "Use of Inverse Gas Chromatography (IGC) to Determine the Surface Energy and Surface Area of Powdered Materials," *Pharm. Res.* 21 (9) pp. 1718–1720 (Letter to the Editor and response by D. Cline and R. Dalby).
Cline, D. and R. Dalby (2002) "Predicting the Quality of Powders for Inhalation from Surface Energy and Area," *Pharm. Res.,* 19 (9) 1274–1277.
Corson, D.R. and P. Lorrain (1962) *Introduction to Electromagnetic Fields and Waves*, W.H. Freeman & Co. San Francisco and London.
Crawford, R., Koopal, L.K., and Ralston, J. (1987) *Colloids and Surfaces*, 27, 57–64.
Criswell, (1973) "Horizon-glow and the motion of lunar dust," in: R.J.L. Grad (ed.) *Photons and Particle Interactions with Surfaces in Space*, Dordrecht, Reidel, Pub. 37, 545–556.
Cundall, P.A. and O.D.L. Strack. "A Discrete Numerical Model for Granular Assemblies," *Géotechnique*, 29, 47–65 (1979).
Debye, P. (1920) *Phys Z.*, 21, 178.
Derjaguin, B.V. (1934) *Kolloid Zeits*, 69, 155–164.
Derjaguin, B.V, V.M. Muller, and Y.P. Toporov (1975) *J. Colloid Interface Sci*, 53, 314–326.
Drego, R.S., G.C. Vogel, T.E. Needham (1971) "A four parameter equation predicting enthalpies of adduct formation," *J. Am. Chem. Soc.*, 93, 6014–6062.
Dupré, A. (1869) in Van Oss, C.J. (1994).
Eco-Snow Systems: www.eco-snow.com a division of BOC Gases, The Linde Group.
Feuerbacher, B., and B. Fitton (1972) Experimental investigation of photoemission from satellite surface materials, *J. Appl. Phys*., 43(4), 1563–1572.
Fowkes, F.F. (1987) "Role of acid-base interfacial bonding in adhesion," *J. Adhesion Sci. Technol*. 1, 7–27.
Frazier, C.E. (2003) "Wood Surface Energy: Wood Quality Parameter?" Virginia Tech, Sept. 25, SEMI Industry Advisory Board Meeting, Blacksburg, VA.
Gady, Barrett, L. (1996) *Measurement of Interaction Forces Between Micrometer-Sized Particles and Flat Surfaces Using an Atomic Force Microscope,* Ph.D. Thesis, Purdue University.
Gady, B.R. Reifenberger, D.S. Rimai, and L.P. DeMejo, (1997) *Langmuir* 13, 2533.
Gady, B.D. Schleef, R. Reifenberger, L.P. DeMejo, and D.S. Rimai, (1996) *Phys Rev B*, 53, 8065.
Gallo, C.F. and Lama, W.L. 1976 "Classical electrostatic description of the work function and ionization energy of insulators," *Institute of Electrical and Electronics Engineers- Transactions*. *On Industry. Applications* 1A–12(1), 7–11.
Grimsey, I.M., J.C. Feeley, and P. York (2002) "Analysis of the Surface energy of Pharmaceutical Powders by Inverse Gas Chromatography," *J. Pharm. Sci*, 91 (2) 571–583.
Grossman, J.J., J.A. Ryan, N.R. Mukerjee, and M.W. Wegner (1970) in *Proceedings of the Apollo 11 Lunar Science Conference*, A.A. Levinson (Ed.), vol. 3, p. 2171. Pergamon Press, New York.
Gutmann, V. (1978) "The donor-acceptor approach to molecular interactions," NY, Plenum Press.
Hamaker, H.C. (1937) *Physica* 4, 1058–1072.
Hausner, H.H. (1967) "Friction Conditions in a Mass of Metal Powder," *Int. J. Powder Metallurgy*, 3(4), 7–13.
Hays, D.A. (1988) in: *Particles on Surfaces 1: Detection, Adhesion and Removal*, K.L. Mittal (Ed.) pp. 351–360, Plenum Press, NY.
Hays, D.A. (1994) "Toner Adhesion," *Advances in Particle Adhesion*, pp. 41–48, D.S. Rimai, and L.H. Sharpe (eds.),
Hays, D.A. (1995) "Adhesion of Charged Particles," *Fundamentals of Adhesion and Interfaces*, pp. 61–71 D.S. Rimai, L.P. DeMejo, and K.L. Mittal (eds.), VSP Utrecht, Netherlands.

Heiken, G.H., D.T. Vaniman, and B.M. French, editors, *Lunar Sourcebook: a User's Guide to the Moon,* Cambridge University Press, 1991(available on CD as LPI Contribution no. 1259, Lunar and Planetary Institute, Houston, TX, ISSN no. 1540–7845).

Hertz, H. (1882) Über die Berührung fester elastische Körper (On the contact of elastic solids), *J. reine und angewandte Mathematik*, 92, 156–171. (for English translation see *Miscellaneous Papers by H .Hertz*, (eds.) Jones and Schott, London, Macmillan, 1896).

Hopkins, M.A., (2004)

Horn, R.G. and D.T. Smith (1992) *Science* 256, 362.

Kaye, B. (1998) Apparatus for determining powder flowability, US Patent 5847294 (issued Dec 8, 1998); also: Kaye, B.H., "Measuring Parameters Relevant to the Flow and Packing of Powder," *Proc. of Respiratory Drug Delivery* V (5), Phoenix, AZ, Apr. 1996 pp. 1–12.

Keesom, W.H. (1921) *Phys Z*., 22, 643.

Israelachvili, J. (1991) *Intermolecular and Surface Forces*, 2nd Ed. Academic Press (Elsevier).

Johnson, K.L., K. Kendall, and A.D. Roberts (1971) "Surface energy and the contact of elastic solids," *Proceedings, Royal Society*, A324, 301.

Johnson, K.L. (1985) *Contact Mechanics*, Cambridge Univ. Press, London.

Lee, L-H. (1995) "Adhesion and cohesion mechanisms of lunar dust on the moon's surface," *Fundamentals of Adhesion and Interfaces*, pp. 73–94. D.S. Rimai, L.P. DeMejo, and K.L. Mittal (eds.), VSP Utrecht, Netherlands.

Leonovich A.K., Gromov V.V., Dmitriyev A.D., Penetrigov V.N., Semenov P.S., and Shvarev V.V. (1974a) The main peculiarities of the processes of the deformation and destruction of lunar soil. In *The Soviet American Conference on Cosmochemistry of the Moon and Planets,* pp. 735–743. NASA SP–370 (1977); also available in NASA Technical Translation F–16034 (1974). [Luna 16 and 20]

Leonovich A.K., Gromov V.V., Semyonov P.S., Penetrigov V.N., and Shvartov V.V. (1975) Luna 16 and 20 investigations of the physical and mechanical properties of lunar soil. In *COSPAR Space Research XV,* pp. 607–616. Akademie-Verlag, Berlin. [Luna 16 and 20]

Lide, D.R., (Ed), CRC Handbook of Chemistry and Physics, 82nd ed., pp. 12–130, CRC Press, Boca Raton, Fla., 2001.

A. Liwo, A.M. Khalili, and H.A. Scheraga (2005) "*Ab initio* simulations of protein-folding pathways by molecular dynamics with the united-residue model of polypeptide chains," *PNAS*, February 15, vol. 102, no. 7, 2362–2367.

London, F. (1930) *Z. Phys. Chem*, 11, 222.

London, F. (1937) *Trans. Faraday Soc*, 33, 8.

Maugis, D., and H.M. Pollock, (1984) *Acta Metall*. 32, 1323.

Mazumder, M.K., R.E. Ware, N. Kaya, and T. Yokoyama, (1990) "Electrical Properties of Powders: Real Time Analysis and Control," Proceedings of Second World Congress on Particle Technology, Sept. 19–22, Kyoto, Japan, Part IV, pp. 505–511.

Mazumder, M.K., D. Saini, A.S. Biris, P.K. Srirama1, C. Calle, and C. Buhler (2004) MARS DUST: CHARACTERIZATION OF PARTICLE SIZE AND ELECTROSTATIC CHARGE DISTRIBUTIONS, Lunar and Planetary Science XXXV 2022.pdf, available at: www.lpi.usra.edu/meetings/lpsc2004/pdf/2022.pdf

McFarlane, J.S., and D. Tabor (1950) "Adhesion of Solids and the Effect of Surface Films," *Proc. Roy. Soc.* A 202, 224–243.

Miller, D.P., D. Lechuga-Ballesteros, L. Williams, T. Tan, J. Kanda, W. Foss, O. Walton, A. Mandel, and X. Cai (2002) "Dispersibility of Spray-dried Raffinose: Effects of Particle Size and Relative Humidity," AAPS Annual Meeting –Nov. 10–14, 2002—Toronto, Canada.

Mitchell J.K., Houston W.N., Scott R.F., Costes N.C., Carrier W.D. III, and Bromwell L.G. (1972) Mechanical properties of lunar soil: Density, porosity, cohesion, and angle of friction. *Proc. Lunar Sci. Conf. 3rd,* pp. 3235–3253.

Mitchell J.K., Houston W.N., Carrier W.D. III, and Costes N.C. (1974) *Apollo Soil Mechanics Experiment S–200.* Final report, NASA Contract NAS 9–11266, Space Sciences Laboratory Series 15, Issue 7, Univ. of California, Berkeley.

Mizes, H.A. (1994) "Surface Roughness and Particle Adhesion," *Advances in Particle Adhesion*, D.S. Rimai and L.H. Sharpe (eds.) Gordon & Breach Pub. pp. 155–165.

Nakagawa, M. (2006) personal communication, Colorado School of Mines, Project Dust.

Newell, H.E. and G. Buckton (2004) "Invers Gas Chromatography: Investigating Whether the Technique Preferentially Probes High Energy Sites for Mixtures of Crystaline and Amorphous Lactose," *Pharm. Res.* 21 (8), 1440–1444.

Pai, D.M. and B.E. Springett (1993) *Rev. Modern Phys*. 65 (1), 163–211.

Pollock, H.M., N.A. Burnham, and R.J. Colton (1994) "Attractive Forces Between Micron-Sized Particles: A Patch Charge model," D.S. Rimai and L.H. Sharpe (eds.) *Advances in Particle Adhesion*, pp. 71–86, Gordon & Breach Pubs.

Pruppacher, H.R., and J.D. Klett, 1997 *Microphysics of Clouds and Precipitation*, 2nd ed. Kluwer, 954 pp.

PurCO_2: www.purco2.com Valencia, CA 91355

Rabinowicz, E. (1965) *Friction and Wear of Materials*, John Wiley and Sons, NY

Rabinovich, Y.J., (2000) *Colloid Interface Sci.* 232, 1.

Rabinovich, Y.J. Adler, M. Esayanur, A. Ata, R. Singh, B. Moudgil (2002) *Adv. Colloid Interface Sci.* 96, 213.

Riddle, F.L. and F.M. Fowkes (1989) "Spectral shifts in acid-base chemistry van der Waals contributions to acceptor numbers," *J. Am. Chem. Soc.*, 112, 3259–3264.

Rimai, D.S., L.P. Demejo, and R.C. Bowen (1994) "The Adhesion of Particles to Polymer Coated Substrates," *Advances in Particle Adhesion*, pp. 139–154, D.S. Rimai and L.H. Sharp (eds.) Gordon and Breach Pub, Amsterdam,.

Rimai, D.S., L.P. Demejo, and R.C. Bowen (1995) "Mechanics of Particle Adhesion," *Fundamentals of Adhesion and Interfaces*, pp. 1–23, D.S. Rimai, L.P. DeMejo, and K.L. Mittal (eds.) VSP.

Rimai, D.S. and D.J. Quesnel (2001) *Fundamentals of Particle Adhesion*, Global Press.

Salisbury, J.W., P.E. Glaser, B.A. Stein, and B. Vonnegut (1964) "Adhesive Behavior of Silicate Powders in Ultrahigh Vacuum," *J. Geophys. Res.* 69, 235.

Schaefer, D.M., M. Carpender, B. Gady, R. Reifenberger, L.P. Demejo, and D.S. Rimai (1995) "Surface roughness and its influence on particle adhesion using atomic force techniques," *Fundamentals of Adhesion and Interfaces*, pp. 35–48.

Schultz, J.L. Lavielle, C. Martin (1987) "The role of the interface in carbon fibre-epoxy composites," *J. Adh.* 23, 45–60.

Schultz, J.L. Lavielle (1989) "Interfacial properties of carbon fibre-epoxy matrix composites," in: D.R. Lloyd, T.C. Ward, H.P. Schreiber, (eds.) *Inverse gas chromatography characterization of polymers and other materials*, ACS Symp. Ser. 391, Washington, DC, Am. Chem. Soc, pp. 185–202.

Sickafoose, A.A., J.E. Colwell, M.Horányi, and S. Robinson (2001) "Experimental investigations on photoelectric and triboelectric charging of dust," *J. Geophysical Res*. vol. 106, no. A5, pp. 8343–8356.

Sickafoose, A.A., J.E. Colwell, M. Horányi and S. Robertson (2002) "Experimental Levitation of Dust Grains in a Plasma Sheath," *J. Geophys. Res.* 107, 27.

Sternovsky, Zoltán, Scott Robertson, Amanda Sickafoose, Joshua Colwell, and Mihály Horányi (2002) "Charging of lunar and Martian Dust Simulants," *Journal of Geophysical Research*, vol. 107, no. E11, 5105, doi:10.1029/2002JE001897.

Stubbs, T.J., R.R. Vondrak, and W.M. Farrell (2006) "A Dynamic Fountain Model for Lunar Dust," *Adv. Space Res*. 37, 59. Also: Vondrak, R.R., T.J. Stubbs, and W.M. Ferrell (2005) "A Dynamic Fountain Model for Dust in the Lunar Exosphere," Workshop on Dust in Planetary Systems 2005, 4071.

Taylor, L.A., H.H. Schmitt, W.D. Carrier III, M. Nakagawa (2005) "The Lunar Dust Problem: From Liability to Asset," *AIAA, 1st Space Exploration Mission*, January 17, 2005

Taylor, L.A. (2005) Personal communication.
Thornton, C. and Z. Ning, (1998) "A theoretical model for the stick/bounce behaviour of adhesive elastic-plastic spheres," *Powder Technology*, 99, 154–162.
Tinsley, B.A., R.P. Rohrbaugh, M. Hei, and K.V. Beard (2000) "Effects of image Charges on the Scavenging of Aerosol Particles by Cloud Droplets and on Droplet Charging and Possible Ice Nucleation Processes, *J. Atmospheric Sci.* 57, pp. 2118–2134.
Todd, P. (2004) "FINAL PROGRESS REPORT on ROBOTIC LUNAR ECOPOIESIS TEST BED," for NASA-NAIC-USRA, Prime Contract NAS5–03110, Research Subcontract 07605–003–020, Space Hardware Optimization Technology, Inc., Greenville, Indiana, 30 April, 2004.
Tomas, J. (2006) "Micromechanics of Particle Adhesion," Fifth World Congress on Particle Technology, Orlando, FL, April 2006, Sessions 75a and 38f. AIChE.
Van Oss, C.J., M.K. Chaudhury, and R.J. Good (1987) "Monopolar surfaces," *Adv. Colloid Interface Sci*, 28, 35–64.
Van Oss, C.J., M.K. Chaudhury, and R.J. Good (1989) *J. Colloid Interface Sci*, 128, 313.
Van Oss, C.J. (1994) *Interfacial Forces in Aqueous Media*, Marcel Decker Inc., NY.
Van Krevelen, D.W. (1976) *Physics of Polymers*, Elsevier, Amsterdam. See also, I.M. Ward, *Mechanical Properties of Solid Polymers*, Wiley, NY, 1990; and J.D. Ferry, *Viscoelastic Properties of Polymers*, Wiley, NY, 1980.
Vinogradov A.P. (1972) Preliminary data on lunar regolith returned by automatic probe "Luna-20." *Geokhimiya,* 7, 763–774.
Walton, O.R. (2004) "Potential discrete element simulation applications ranging from airborne fines to pellet beds," *SAE 2004 Transactions J. Aerospace* paper 2004–01–2329 (paper available at: www.grainflow.com).
Walton, O.R., C.P. De Moor, D.P. Miller, (2003) "Simulation of Low-Stress Compaction of Cohesive Micron-Scale Powders," AIChE 2003 Annual Meeting, Nov. 16–21(Session T4–35a), San Francisco, CA.
Whipple, E.C. (1981) "Potentials of surfaces in space," *Rep. Prog. Phys*., vol. 44, pp. 1197–1250.
Wolf, D.E., T. Unger, D. Kadau, L. Brendel (2005) "Compaction of Cohesive Powders," *Powders and Grains*, eds. R. García-Rojo, H.J. Herrmann, S. McNamara (Balkema, Leiden) p. 525.
Wu, W., R.F. Griese Jr., and C.J. van Oss (1996) *Powder Technology*, 87, 129–132.
Young, T. (1805) in Van Oss, C.J. (1994).
Zhang, X. and L. Vu-Quoc (2002) "Modeling the dependence of the coefficient of restitution on the impact velocity in elasto-plastic collisions," *Int'l. J. Impact Eng*. 27, 317–341.

Appendix A—Bulk Powder Physical Properties (Cohesion, Cohesivity, Flowability)

A limited number of particle-scale measurements have been done on the physical properties of lunar regolith particles that contribute to inter-particle cohesion, like surface energy, hardness, surface morphology. On the other hand, a significant number of bulk soil mechanics tests have been performed on Lunar soil, including penetrometer, direct shear, one-dimensional oedometer, and triaxial tests. Several of these tests have indicated that lunar soil exhibits a measurable *cohesion*. Most of these tests were interpreted in terms of the classic Mohr-Coulomb equation, relating shear-stress, τ, to normal-stress, σ

$$\tau = c + \sigma \tan \varphi_f \tag{A1}$$

where the parameter, φ_f, is known as the *friction angle* (or *internal-angle-of-friction*), and the zero-normal-stress intercept, c, is known as the *cohesion* (or *cohesive strength*) of the soil. Unfortunately, while the Mohr-Coulomb relation is a reasonable representation of the response of a particular sample starting at a particular consolidation, it is not a unique fundamental material property. A typical soil can exhibit a family of Mohr-Coulomb curves, each one unique to a particular degree of pre-consolidation. Thus, the values of the fitting parameters, c, and φ_f depend on the previous consolidation of the soil sample. As outlined in the Lunar Sourcebook (at least for one basaltic stimulant of lunar soil) the range of values of c from 0.03 to 3 and φ_f from 28° to 55° can all be correlated with the *relative-density* (see fig. A1 [e.g., fig. 9.27 *Lunar Sourcebook*, after Mitchell et al. 1972, 1974]) where *relative-density* is the percent of compaction between the *minimum bulk density* (the lowest bulk density "at which the soil can be placed") and the *maximum bulk density* "at which the soil can be placed". The "best-estimate" value for cohesion of Surveyor soils was 0.35 to 0.70 kPa, while cohesion values for Apollo 12 samples ranged from 0.1 to 3.1 kPa depending on the initial degree of consolidation. The Apollo Model 'best estimate' for lunar soil cohesion was 0.1 to 1.0 kPa, with the friction angle ranging from 30° to 50°.

Several researchers have indicated a need to understand the high cohesion evidenced by the stability of steep slopes and trench walls observed in lunar exploration missions [e.g., Lee, 1995, Taylor, 2005]. As described in the Lunar Sourcebook [Heiken, et al., 1991] soil-mechanics based stability analysis would predict that "a vertical cut can safely be made in lunar soil to a depth of about 3 m, while an excavated slope of 60° can be maintained to a depth of about 10 m." Given the reduced driving force of lunar gravity, these predictions are not unusual for a material with the size-distribution of lunar regolith and with the degree of consolidation found in-situ. It is primarily the pre-exiting state of consolidation that is surprising, and which results in the observed cohesive strength [as supported by the tests on JSC–1 samples described previously].

A word or two about terminology may be beneficial to the reader, especially since researchers in different specialties use the same words to mean different things relating to material properties. *Interparticle friction* contributes to the shear resistance of a granular material, however, the soil-mechanics quantity *friction-angle*, φ_f, is not a direct measure of *interparticle friction*. It is simply the arctangent of the slope of the shear-stress normal-stress line for a material obeying a Mohr-Coulomb relation, equation (A1). Similarly, the unconfined shear strength, or the c intercept of the Mohr-Coulomb curve, is nonzero for *cohesive* materials; however, c is not a direct measure of the interparticle cohesive force or energy. Nonetheless, the fact that lunar regolith exhibits a measurable soil-mechanics cohesion, is a good indication that interparticle cohesive forces are significant for that material.

The cohesive behavior of a dry powder or its *cohesiveness* or *cohesivity* is less well defined than the *cohesion* or *cohesive-strength* (i.e., c in eq. (A1)). Generally a powder is said to exhibit cohesive behavior when it fails to flow like dry sand, or agglomerates, or clumps, or exhibits shear-strength properties somewhat like a solid. As one example, the Aero-Flow avalancher [Kaye, 1998] determines cohesive behavior by analyzing the random nature of the time sequence of clumping avalanches in a slowly rotating horizontal cylinder, partially filled with powder. A variety of other measures also exist for

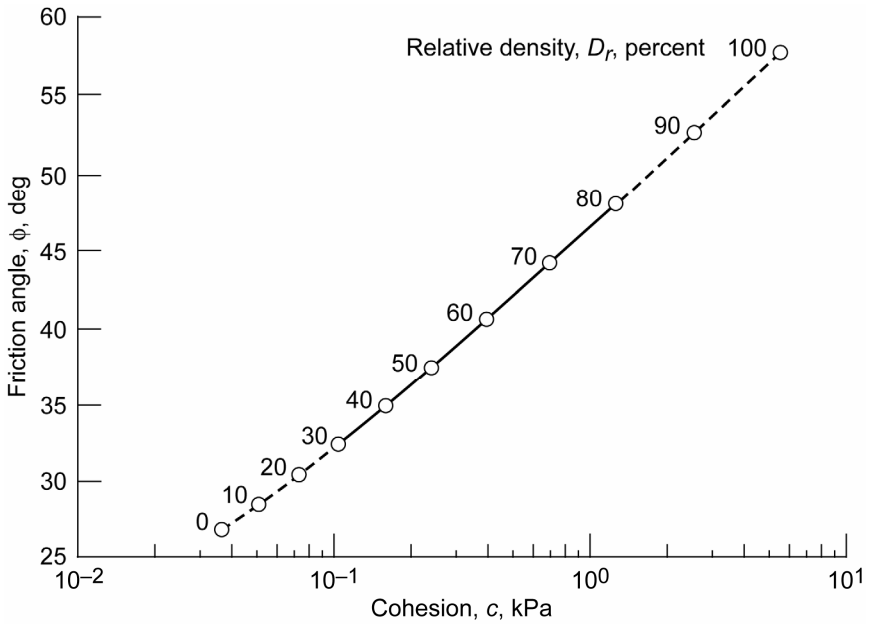

Figure A1.—Measured shear strength of a basaltic simulant of lunar soil, showing the friction angle (verticle axis) and cohesion (horizontal axis) for different relative densities (after Mitchell et al. [1972 and 1974]). Taken from Heiken et al. [1991].

flowability or cohesiveness. In almost all of them the "measurement" of cohesive behavior is really an evaluation of a measurement *system*, usually involving a container of a specific size, a specific driving force (often gravity) and a specific type of flow "expected" (if the material were not *cohesive*). If the size of the container changes, the driving force changes, the type of flow examined, or the material properties change, then the characterization of the powder's *cohesiveness* or *flowability* may be different.

The *compressibility* of a powder is often associated with its cohesiveness and has formed the basis for a variety of index tests for ranking the *cohesiveness* or *cohesivity* of fine powders. Cohesive powders existing in low-density "sifted" states, are quite compressible, and can easily be compacted to higher densities by external loads, or by handling or jarring their containers. The pharmaceutical industry routinely deals with fine cohesive powders and often characterizes how cohesive a powder is by its Hausner ratio, that is, the ratio of the density after being "tapped" repeatedly (up to thousands of times in a controlled tapped-density test) to initial sifted density [Hausner, 1967; Abdullah and Geldart, 1999]. Such tapped-density tests serve as index tests to classify the cohesiveness of powders. For a more device-independent measurement of cohesive powder compaction, the stress *versus* density behavior under controlled uniaxial or isotropic compression can be measured. Figure A2 compares the solids fraction as a function of axial stress during uniaxial compaction of fine, cohesive powders comprised of nearly spherical raffinose particles made by spray drying an aqueous solution with different mass fractions of raffinose, ranging from 0.05 to 15 percent [Walton, et al., 2003; Miller et al., 2002] and similar compaction (oedometer) data for Russian lunar regolith samples Luna 16 and 20 [Leonovich et al., 1974, 1975, in Carrier et al., 1991]. The Luna samples are comprised of typical nonspherical, angular, regolith with perhaps a somewhat higher fraction of agglutinates than most Apollo samples. They were not as fine nor as cohesive as the raffinose, however, they did exhibit an unusually low initial solids fraction—a feature often associated with very cohesive powders (although there is some speculation that the low solids fraction of the Luna samples is due to their unusually high agglutinate content [Nakagawa, 2006]).

The median particle size for the raffinose powders shown in figure A2 ranged from approximately 0.8 μm to ~4 μm. As seen in this figure, the initial solids fraction of the raffinose powder ranged from 10 to 25 percent, and each powder compacted by a factor of from 2.5 to 4 in going from 0.01 to 1 *Bar* pressure. The particles in the raffinose samples of figure 2 are particularly cohesive, and they also have relatively large contact-spot areas when they "touch" neighboring particles because they are nearly spherical.

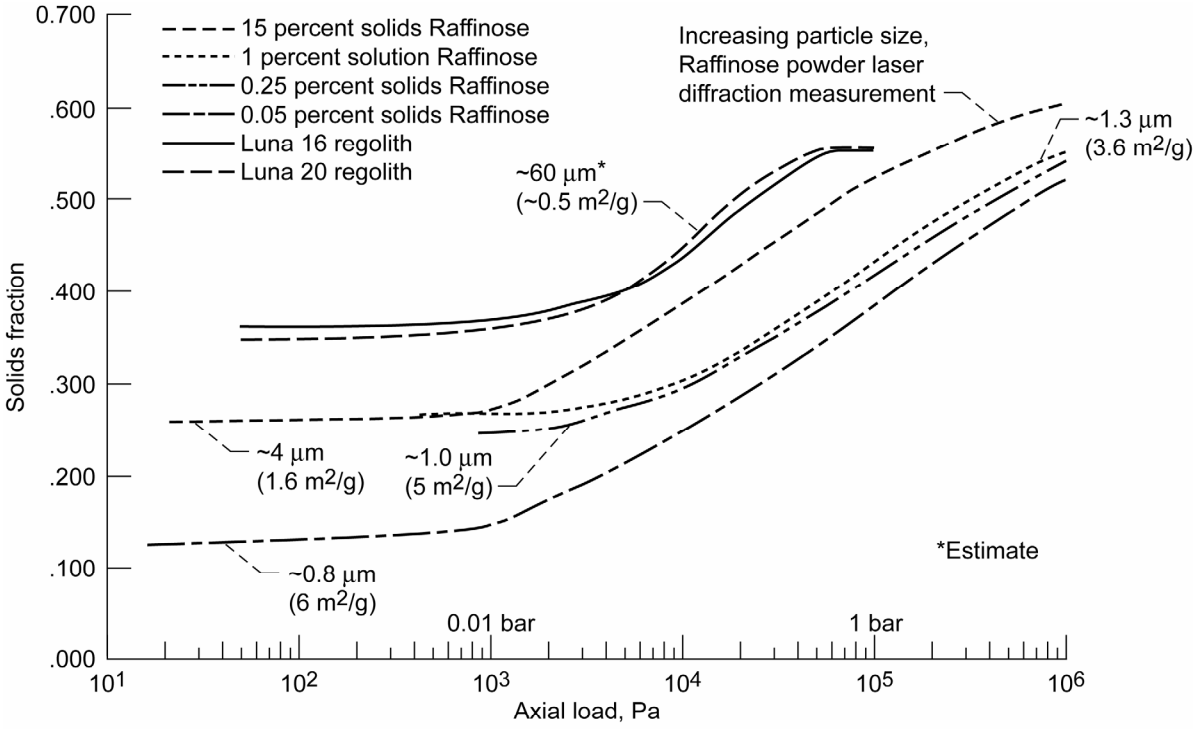

Figure A2.—Uniaxial compaction of cohesive powders. Horizontal portion at left end of each curve is likely reloading to conditions under which sample was preared [any unloading-reloading would occur alone nearly horizontal lines branching to the left off of each curve]. The knee to less com- pressible behavior at high pressure probably indicates a change in the mode of deformation (i.e., possibly changing from collapse of an initially 'open' structure by particle rearrangement, to a more-usual compact configuration where futher compaction occures by much smaller-scale particle rearrangement, or by particle deformation or damage). Compaction has nearly ceased by 1-bar load for the regolith, but would be expected to resume at higher loadings as porous particles fracture and crush [Leonovich, et al., 1974 and 1975; Miller et al., 2002; and Walton et al., 2003].

Appendix B—Surface Energy Measurement

Measurement of the surface energy of solids is most often accomplished by determining the adhesive interaction energy between the solid surface in question and a probe material (usually a liquid or gas) with well characterized properties. As previously mentioned, the intermolecular forces collectively known as the van der Waals forces, all decay with distance, d, as d^{-6}, and originate from: a) fluctuating dipole/induced-dipole (or dispersion) interactions, described by London [1930, 1937]; b) randomly orienting-dipole/induced-dipole (or induction) interactions, described by Debye [1920]; and randomly orienting-dipole/dipole (or orientation) interactions, described by Keesom [1921]. All atoms exhibit London-dispersion interactions. Keesom and Debye interactions are only found among molecules which have permanent dipole moments.

In addition to the collective van der Waals forces, materials in contact can interact by other weak bonding interactions through electron donor-receptor (Lewis acid-base) interactions. These acid-base interactions contribute to measured surface energy values and can be selectively identified through the use of appropriate liquid or gaseous probes. Nonpolar probe liquids or gases are used to measure the dispersive part of the van der Waals forces, while other probes can indicate contributions from both polar and acid-base interactions at interfaces. Contributions to interfacial energy beyond the dispersive term, γ^D, (probed with nonpolar molecules) are usually collectively referred to as "polar" contributions to the surface interaction energy (and usually categorized as either electron "acceptor" γ^+, or "donor" γ^-, contributions to the interaction energy).

Contact Angle

The surface tension of a liquid can be readily measured. The surface energy (per unit area) of a solid can be shown to be analogous to the surface tension of a liquid, but it is not as straightforward to measure. Contact angle measurements, first described by Thomas Young [1805], remain at present, among the simplest and most accurate methods for characterizing the surface properties and determining the interaction energy between a liquid, L, and a solid, S, at the minimum equilibrium distance [van Oss et al., 1989]. Young showed that the contact angle, θ, for a submerged air bubble attached to a solid surface, can be related to the surface tension of a liquid, γ_L, the surface energy of a solid, γ_S, and the interfacial tension between the solid and liquid, γ_{SL}, by,

$$\gamma_L \cos\theta = \gamma S - \gamma_{SL} \tag{B1}$$

Dupré [1869] showed that the change in the free energy associated with bubble-solid adhesion is given by,

$$\Delta G_{SL} = \gamma_{SL} - \gamma_{SL} - \gamma_S - \gamma_L \tag{B2}$$

Combining equations (B1) and (B2) we have,

$$-\Delta G_{SL} = \gamma_L (1 + \cos\theta) \tag{B3}$$

which is known as the Young-Dupre equation. For liquids and solids consisting of nonpolar molecules, the interaction free energy,

$$\Delta G_{SL} = 2\sqrt{\gamma_S^D \gamma_L^D} \tag{B4}$$

(where the superscript, D, refers to the dispersive contribution to the surface energy of each material, i.e., the nonpolar part of the van der Waals interaction at "contact").

A variety of methods exist to measure contact angles between liquids and solids (and powdered solids). The value of the contact angle, θ, is a measure of the competing tendencies between the energy of cohesion of the liquid molecules and the energy of adhesion between the liquid and solid. When the work

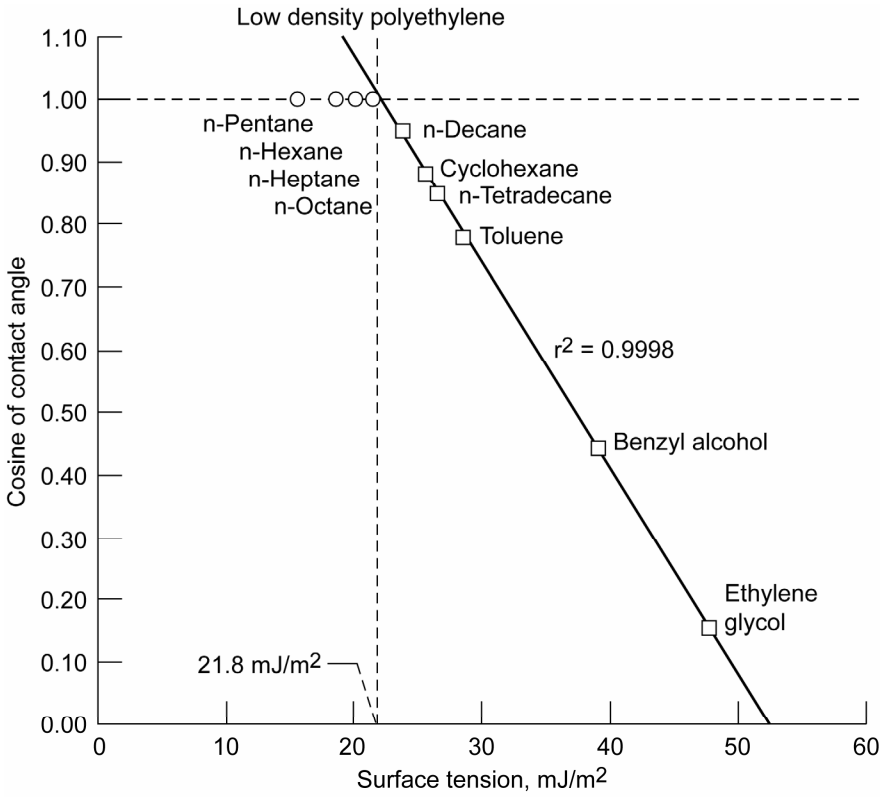

Figure B1.—Zisman method to determine solid surface energy from the contact angle of drops (Sissile drop technique) of various liquid probes on the surface [Frazier, 2003].

of cohesion between liquid molecules exceeds the work of adhesion between a solid and a liquid, a drop of liquid placed on the solid surface forms a finite contact angle. If the work of adhesion is higher than the work of cohesion, spreading occurs. With a single contact angle measurement the interaction energy, ΔG_{SL}, between the liquid and solid can be determined. If the surface energy (tension) of the liquid is known, then the surface energy of the solid can be calculated (using eq. (B4)). Alternatively, the cosine of the contact angle for various probe liquids can be graphed against their known surface tension values to find the zero-contact-angle intercept corresponding to the surface tension of a liquid whose surface energy exactly matches the surface energy of the solid (the Zisman method). Figure B1 [Frazier, 2003] shows a representative graph of the cosine of the contact angle versus surface tension for a series of nonpolar alkane probe liquids (among other liquids) on a low-density polyethylene surface (For comparison the surface tension of water is approximately 73 mJ/m^2).

For interfaces involving polar liquids and solids, the interaction energy includes additional terms usually associated with electron acceptor (acid), γ^+, or electron donor (base), γ^-, components to the surface free energy or surface tension. The total interaction energy is the sum of the dispersive (nonpolar) interaction energy and any nonzero polar interaction energy terms,

$$\Delta G_{SL} = -2\sqrt{\gamma_S^D \gamma_L^D} - 2\sqrt{\gamma_S^+ \gamma_L^-} - 2\sqrt{\gamma_S^- \gamma_L^+} \tag{B5}$$

If the dispersive and polar properties of various “probe” liquids are known, then three measurements can be made (with different probe liquids), to produce three equations which can be solved to determine the three components of the surface energy of the solid, γ_S^D, γ_S^+, and γ_S^-.

Other, ostensively-equivalent methods exist to determine the 'contact' angle for probe liquids on solids from, for example, the height of rise, h, of a liquid of density, ρ_L, on a vertical plate (Wilhelmy Plate method [Adamson, 1990]),

$$1-\sin\theta=\frac{h^2\rho_L g}{2\gamma_L} \tag{B6}$$

where g is the acceleration of gravity. For solids that exist only in powdered form, there are alternative methods such as *capillary rise* [Adamson, 1990] and *thin layer wicking* (based on the velocity at which liquid creeps up a slide with a previously dried layer of powder has been deposited) [Crawford, et al., 1987]. Alternatively, the contact angle for powders can be obtained from the heat of immersional wetting in various testing liquids (e.g., water, formamide, etc.) in a microcalorimeter. In the immersion technique, a powdered sample is usually degassed to remove pre-absorbed water and then immersed in liquid [Wu et al., 1996].

The contact angle determination techniques described above are widely used in the mineral and chemical industries to characterize the properties of solid and powder surfaces. In recent years another technique for measuring the surface energy of fine powders based on gas adsorption in the infinite dilution limit, inverse gas chromatography, IGC, has been gaining acceptance.

Inverse Gas Chromatography (IGC)

IGC has been in existence for nearly 20 years, and, over the past decade, has seen active development as a powder characterization method, especially in the pharmaceutical industry where many powders of interest are soluble in various liquids. The IGC nonpolar probe gas results are usually interpreted [Grimsey, et al., 2002] according to the approach described by Schultz and Lavielle [1989], or, Schultz et al., [1987]. In Schultz' approach, a series of *n*-alkanes are used to determine the dispersive component, γ_S^D, while the specific component, ΔG_A^{SP}, of the free energy of adsorption is determined using polar probes. For the alkanes, the measured retension volume, V_N, is related to the dispersive component by,

$$RT\ln V_N = a\sqrt{\gamma_L^D}\,2N\sqrt{\gamma_S^D}+C \tag{B7}$$

where, a, is the interaction surface area (of the powder in the IGC column), γ_L^D is the dispersive free energy of the probe, N is Avagadro's Number, and R is the gas constant.

The dispersive component, γ_S^D, of the free energy of the surface is then calculated from a graph of $RT\ln V_N$ versus $a\sqrt{\gamma_L^D}$ as shown in figure B2.

Surface energy contributions from sources other than the dispersion (London interaction) component are determined using various polar probe vapors (such as Tetrahydrofluran, THF, and chloroform) which interact with polar as well as dispersive forces, and are usually interpreted according to a theory developed by Gutmann [1978] and Drago et al. [1971] applied to interfaces (Fowkes [1987], van Oss [1987]). Gutmann numbers describe the electron donor or base, *DN*, and electron acceptor or acid, *AN*, properties of liquids. *AN* was corrected to take into account dispersive contributions by Riddle and Fowkes [1989] to give *AN**. The specific component of surface free energy, ΔG_A^{SP}, is related to the electron donor, K_D, and electron acceptor K_A parameters on the surface by

$$\Delta G_A^{SP} = K_A DN + K_D AN* \tag{B8}$$

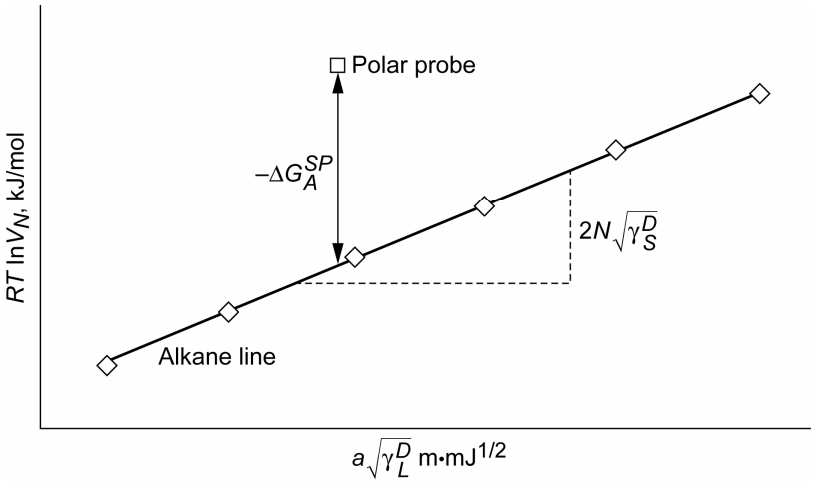

Figure B2.—Determination of surface energy (polar and dispersive components) using inverse gas chromatography (IGC) (after Grimsey et al. [2002]).

By measuring the values of ΔG_A^{SP} for several probe vapors, and plotting *DN/AN** against ΔG_A^{SP}/AN*, the values for K_A and K_D can be calculated for a powder of interest.

IGC analysis is quite time consuming. Columns are typically left 12 to 24 *h* to equilibrate under the flow of the carrier gas. The method employs the infinite dilution regime for the probe gas concentration wherein the net retention volume is independent of the quantity of probe injected and the elution peaks are essentially Gaussian. A minimum of five probes are necessary to determine the surface parameters (three alkanes an acidic probe and a basic probe) and it is recommended that [Grimsey et al., 2002] each probe be injected three times in order to provide a measure of the reproducibility and to ensure that the nature of the surface is not changing during the measurements. Time is also necessary between each probe to make sure that the previous molecules have eluted before the next probe is injected. Even with auto injection systems a typical test can take more than 30 *h*.

The IGC method might be considered as a "developing" technology, since there still are current papers describing improvements in interpretation of results, refinements in methods and protocols for measurement of surface properties, and uncertainties in reference values for the alkane probe gases. One concern with the analysis method (described above) is that, while the dispersive part of the surface energy, γ_S^D, is determined in energy per unit area (mJ/m^2) and can be compared directly with other measurements from other methods (e.g., see Newell and Buckton, [2004]), the polor component (using the Gutmann number analysis) usually produces a nondimensional ratio of K_D/K_A, to describe the polar nature of the surface, which cannot be compared directly with other polar probe measurement results. There are active discussions in current literature on both method interpretation and improvements. The reader is referred to recent papers (Ahfat et al., [2001], Grimsey et al., [2001], Cline and Dalby [2002], Chow et al., [2004], Newell and Buckton [2004], Voelkel [2004], all available electronically) for discussions on IGC developments. For example, as part of the IGC measurement it is necessary to determine the surface area being probed by the test gases. Until recently this was usually accomplished by a separate specific surface area measurement (BET analysis using a separate instrument and inert probe gases) or utilized a large extrapolation from the alkane probe gas measurements. Newell and Buckton [2004] describe a method to perform BET analysis on the powder sample using a series of increasing concentration injections in the same ICG apparatus (and with the same powder sample) as used for the surface energy characterization. They also explore whether or not the infinite-dilution gas flows in IGC "preferentially" probe high-energy sites on heterogeneous surfaces. Voelkel [2004] reevaluates analysis protocols and the literature values for the reference probe alkanes to improve accuracy of ICG results.

Appendix C—JKR Model Details

The JKR model has been verified experimentally for large relatively soft bodies for which surface deformations are larger than any asperities, so that the model assumption that the surfaces are smooth is not violated. The JKR model assumes that the interfacial forces have zero range before contact, and, in the usual application of the JKR model for cohesive contacts, the approximately 4 nm range of those forces is, indeed, small compared to the other displacements involved. In the JKR model the total force, F, acting between two contacting bodies and the relative displacement between them, α, are given by the following equations,

$$F = \frac{4E^* a^3}{3R^*} - (16\pi\gamma E^* a^3)^{1/2} \tag{C1}$$

$$\alpha = \frac{a^2}{R^*} - \left(\frac{4\pi\gamma a}{E^*}\right)^{1/2} \tag{C2}$$

where, a is the contact spot radius, γ is the surface energy per unit area, R^* is the effective radius of the contacting bodies at the contact point, and E^* is the effective modulus,

$$\frac{1}{E^*} = \frac{1-\nu_1^2}{E_1} + \frac{1-\nu_2^2}{E_2} \tag{C3}$$

Figure C1 shows the force-displacement relations for a noncohesive, elastic Hertzian contact [Hertz, 1882] and the JKR model. Using this figure as a schematic salient features of the models can be described. As particles approach, the force is zero for either model, and we move along the horizontal axis towards the origin from the left. As the particles touch (and α becomes positive) the noncohesive Hertzian model gradually builds up a repulsive (positive) force that increases with the 3/2 power of α. When contact first occurs (at $\alpha = 0$) in the JKR model, the surfaces snap together, with a net attractive force, going from the origin to point A. Then as the particles continue to approach each other, the force moves to a net zero value at point B, and then becomes repulsive (e.g., in traversing the path to point D). Upon unloading, the JKR force retraces from point D, through points B and A, and then continues (with negative α and negative force values) to points C and S, at which point the surfaces snap apart and the force returns to zero. The distance from point A to S represents outward elastic deformation of the particle surfaces as the particles are pulled apart, but before final separation occurs. The minimum in the force-displacement relation corresponds to the pulloff force, F_c, is given by,

$$F_c = -3\pi\gamma R^* \tag{C4}$$

With no applied load the particles are ‘pulled’ together by the cohesive force causing some deformation in the contact region. The point where the JKR curve crosses zero (point B) represents the equilibrium point with no applied loads. If applied forces pull the contacting bodies apart, they adhere to one another, deforming the surfaces outward. Final separation occurs at a (negative surface) displacement, α_s, given by,

$$\alpha_s = -3\left(\frac{\pi^2\gamma^2 R^*}{16E^{*2}}\right)^{1/3} \tag{C5}$$

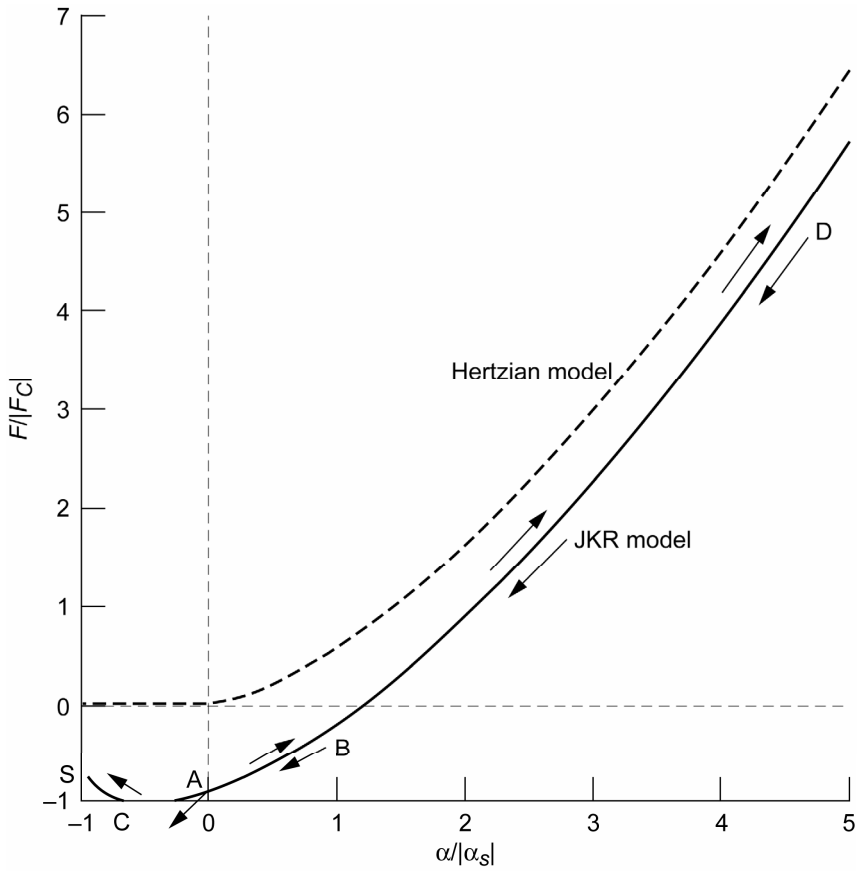

Figure C1.—Force-displacement relations for cohesive JKR model, and linear elastic Hertzian model [Mei, 2000].

The mathematical form of the force-displacement relation in the JKR model has been experimentally verified for macroscopic gelatin spheres [Johnson, 1985] and at the AFM (i.e., nanometer) scale [Burns et al., 1999].

Plastic Deformation at Contact Points

The contact area predicted by Hertzian (linear-elastic) theory for contacts between smooth spheres, and for elastic JKR model spheres is usually quite small compared to the particle size. Consequently, the total force is concentrated in such a small area that the stresses can exceed the elastic limit of the materials, even while the total force is quite low. Finite element calculations of the distribution of normal direction stress in the contact area, between perfectly elastic spheres, reproduce Hertz' theoretical hemispherical shape. If the peak normal stress exceeds 1.6 Y, where Y is the yield strength, then plastic deformation starts [Johnson, 1985]. Finite element calculations using an elastic-plastic material model show that the stress distribution flattens and covers a larger area than the Hertzian elastic model prediction. Figure C2 shows the stress distribution in the contact region between two spheres for both an elastic (Hertzian) and an elastic-plastic material model [Zhang, 2002].

Careful examination of the physics involved with micron-scale particles indicates that plastic deformation is likely at contacts between particles, even if no external loads are applied. One interpretation of the JKR model is to take the two terms for the normal force in equation (C1) as literally representing the total compressive and attractive forces acting between two JKR model spheres. Based on this assumption the compressive load is given by the positive term in equation (C1). With no applied load, F is zero, and the two terms on the right hand side of equation (C1) cancel. At that point the repulsive

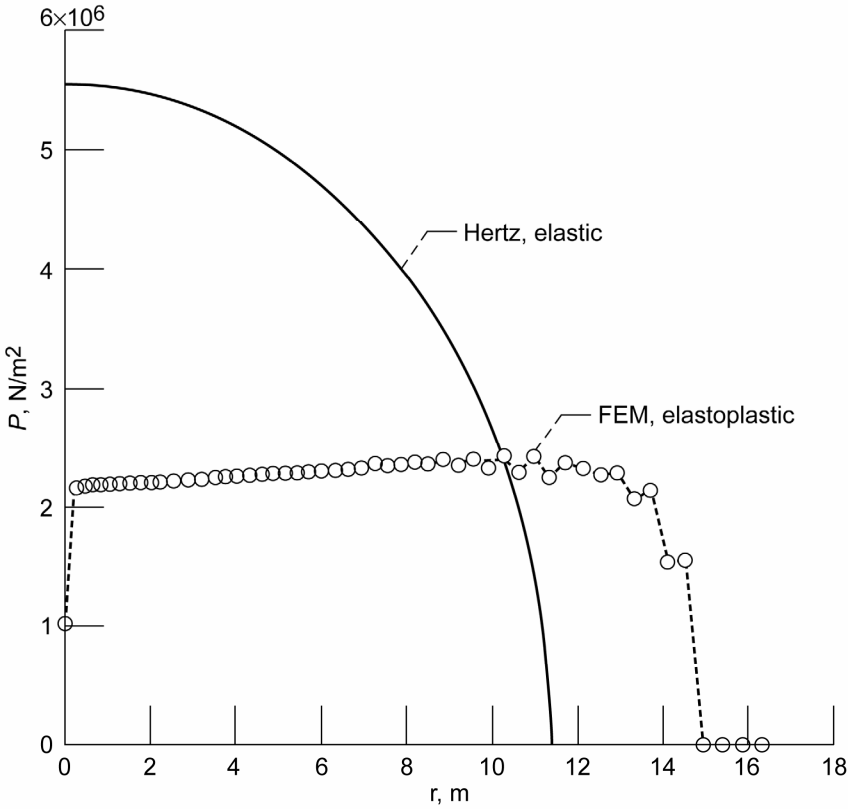

Figure C2.—Normal stress distribution for contact region of elastic (Hertz) contact, and for an elastoplastic (FEM) contact with $P \sim 40P_y$ [Zhang, 2002].

force, $F_0 = 12\pi\gamma R^*$, is four times the pull off force, F_c. This zero-applied-load repulsive force, F_0, scales linearly with the particle size, while the load for onset of yield, F_Y, for two equal sized elastic spheres pressed together, varies with the square of the particle size (Hertzian), [Johnson, 1985]

$$F_Y = \frac{\pi^3 R^2 (1-\nu^2)^2}{6E^2}(1.6)^3 Y^3 \tag{C6}$$

Thus, as particle size decreases, the value of F_0 will exceed F_Y for all radii below some threshold radius, R_{0Y}. Particles smaller than R_{0Y} (or with a radius of curvature at the contact point less than R_{0Y}) will experience plastic deformation at cohesive contacts with neighboring particles, simply due to the attractive forces (without any applied external loads).

The literal interpretation of the terms in the JKR force displacement expression, equation (C1), as representing the true adhesive and repulsive portions of the total force, is probably not correct (and has little experimental evidence for support—only the total JKR force-displacement curve has been confirmed experimentally, not the individual terms). Maugis and Pollock [1984], noted that the force displacement relation for the JKR model is quite close to a Hertzian force-displacement curve that has been shifted (down) by an amount $F_c = -3\pi\gamma R^*$. [Note: an examination of the curves in figure C1 might indicate that a more precise analysis could be based on both a horizontal and a vertical shift of the Hertzian curve by amounts $-\alpha_s/2$ and $-F_c$, respectively, to better approximate the JKR curve].

As an alternative to taking the individual terms of the JKR model as literally indicating the attractive and repulsive parts of the total force, one could set $F_c \approx F_Y$ in equations (C4) and (C6) to obtain a rough indication of the particle size, R_{cY}, below which plastic deformations would be expected, even with no

external loads at the contact. For this estimate we can also set, $Y \approx 0.003E$, and select a Poisson ratio of $\nu = 0.3$, for the sake of illustration.

$$F_Y = \frac{\pi^3 R^2 (1-\nu^2)^2}{6E^2}(1.6)^3 Y^3 \approx F_c = -\frac{3}{2}\pi\gamma R \tag{C7}$$

Rearranging and substituting approximate values for Y and ν, we obtain,

$$R_{cY} \approx 1\times 10^7 \frac{\gamma}{E} \tag{C8}$$

See table 1 in the text for representative values substituted into equation (C8).

In the limiting case of fully plastic contacts the Maugis and Pollock (MP) theory models the normal stress as nearly constant over a circular contact spot of radius, a, and the total normal force, F_N, consisting of both an applied load F_A plus an adhesive force $2\pi W_a R$ is balanced by a constant compressive stress, σ_p, over the contact spot area,

$$F_N = F_A = 2\pi W_a R = \pi\sigma_p a^2 \tag{C9}$$

where the plastic stress approaches a constant value $\sigma_p \approx 3Y$. In the absence of any applied external load, equation (C9) reduces to,

$$a = [2W_a R/3Y]^{\frac{1}{2}} \tag{C10}$$

[A slight inconsistency in the MP model, of using an adhesive force based on an undeformed sphere, $2\pi W_a R$, combined with an assumed contact spot size that is based on a deformed plastic region with uniform stress, $\pi\sigma_p a^2$, does not appear to negate some of the success of the model, as described below].

For comparison, the JKR model (based on elastic deformations only) predicts that the contact radius with no applied load (i.e., point B in fig. C1) is given by,

$$a^3 = \frac{9W_a \pi R^2 (1-\nu^2)}{2E} \tag{C11}$$

Particle Engulfment Limit for Contacts with Soft Substrates

When particles are in contact with relatively soft substrates it is possible for the adhesive forces to cause the particles to "sink" into the substrate and become totally engulfed. Ramai et al., [1994] studied this phenomenon by adding plasticizer to polymers to reduce the Young's modulus and yield strength. They measured the contact radius of nominally 4 and 11 μm glass beads placed on the soft polymer surfaces, and determined if the size of the contact spot varied with the particle-radius to the 2/3 power (consistent with the elastic JKR theory, i.e., equation (C11)) or with the particle-radius to the 1/2 power (consistent with the MP, fully plastic contact model, i.e., equation (C10)). With small amounts of plasticizer (~5 percent) Ramai et al. found the contact spot size varied with the bead radii to the 1/2 power, consistent with MP theory for fully plastic contacts. When the plasticizer fraction was increased to 10 percent, interestingly, the resulting very soft and rubbery polymer exhibited larger contact spot sizes which varied with the 2/3 power of the glass beads consistent with elastic deformation in the contact region. One rather interesting observation found in these studies was that if either the yield strength or the modulus of the substrate is small enough for the diameter of the contact spot (predicted by either JKR or MP theory) to exceed the particle diameter, it is possible for the particle to become totally

engulfed by the substrate, just due to the effect of adhesive surface forces, with no external loads. Since the predicted contact spot sizes decrease more slowly than the particle size for either model, such an observation reinforces the desirability of using hard coatings to avoid entrapment or lodging of very fine particles in surfaces. For contacting materials that are in the elastic regime (i.e., obeying the JKR model, the critical radius, R_c, at which engulfment might occur is given by [Rimai, et al., 1995]

$$R_c \approx {}^{7\gamma_{12}}\!/_{E} \tag{C12}$$

Alternatively, for contacts which are fully plastic, and describable by the MP model,

$$R_c \approx {}^{2\gamma_{12}}\!/_{3Y} \tag{C13}$$

For very soft materials these relations can be used to evaluate whether the contact size is approaching the particle size for very small dust particles—which could indicate potential for particles becoming deeply embedded in (and/or engulfed by) a soft substrate material.

REPORT DOCUMENTATION PAGE		Form Approved OMB No. 0704-0188

1. REPORT DATE *(DD-MM-YYYY)*	2. REPORT TYPE	3. DATES COVERED *(From - To)*
18-04-2007	Final Contractor Report	

4. TITLE AND SUBTITLE
Adhesion of Lunar Dust

5a. CONTRACT NUMBER
NNC06VC87P

5b. GRANT NUMBER

5c. PROGRAM ELEMENT NUMBER

6. AUTHOR(S)
Walton, Otis, R.

5d. PROJECT NUMBER

5e. TASK NUMBER

5f. WORK UNIT NUMBER
WBS 092837.04.02.03

7. PERFORMING ORGANIZATION NAME(S) AND ADDRESS(ES)
Grainflow Dynamics, Inc.
1141 Catalina Drive
PMB #270
Livermore, California 94550

8. PERFORMING ORGANIZATION REPORT NUMBER
E-15840

9. SPONSORING/MONITORING AGENCY NAME(S) AND ADDRESS(ES)
National Aeronautics and Space Administration
Washington, DC 20546-0001

10. SPONSORING/MONITORS ACRONYM(S)
NASA

11. SPONSORING/MONITORING REPORT NUMBER
NASA/CR-2007-214685

12. DISTRIBUTION/AVAILABILITY STATEMENT
Unclassified-Unlimited
Subject Category: 91
Available electronically at http://gltrs.grc.nasa.gov
This publication is available from the NASA Center for AeroSpace Information, 301-621-0390

13. SUPPLEMENTARY NOTES
Project manager, Allen Wilkinson, Microgravity Division, NASA Glenn Research Center, organization code RUF, 216-433-2075.

14. ABSTRACT
This paper reviews the physical characteristics of lunar dust and the effects of various fundamental forces acting on dust particles on surfaces in a lunar environment. There are transport forces and adhesion forces after contact. Mechanical forces (i.e., from rover wheels, astronaut boots and rocket engine blast) and static electric effects (from UV photo-ionization and/or tribo-electric charging) are likely to be the major contributors to the transport of dust particles. If fine regolith particles are deposited on a surface, then surface energy-related (e.g., van der Walls) adhesion forces and static-electric-image forces are likely to be the strongest contributors to adhesion. Some measurement techniques are offered to quantify the strength of adhesion forces. And finally some dust removal techniques are discussed.

15. SUBJECT TERMS
Dust; Adhesion forces; Lunar soil; Surface energy

16. SECURITY CLASSIFICATION OF:			17. LIMITATION OF ABSTRACT	18. NUMBER OF PAGES	19a. NAME OF RESPONSIBLE PERSON
a. REPORT	b. ABSTRACT	c. THIS PAGE			Allen Wilkinson
U	U	U		45	19b. TELEPHONE NUMBER *(include area code)* 216-433-2075